The simultaneous conversion and storage of solar energy into rechargeable batteries by a photo-assisted charging strategy

September 2017

LI QI

The simultaneous conversion and storage of solar energy into rechargeable batteries by a photo-assisted charging strategy

Graduate School of Systems and Information Engineering

University of Tsukuba

September 2017

LI QI

ABSTRACT

Rechargeable batteries have been considered as a promising generation for the renewable energy storage due to the high specific energy and power, long cycle life and so on. The utilization of solar energy into the rechargeable battery, provides a solution to not only greatly enhance popularity of solar energy, but also save the input electric energy for the conventional rechargeable battery. In particular, the development on the photoassisted rechargeable batteries with the internal integration of photoelectrode will simplify the storage system and deliver the high capacity similar with that of conventional battery. This concept has been demonstrated via converting and storing of solar energy into various rechargeable batteries.

Based on the faster diffusion of ions or elections in the aqueous than the organic solution, an aqueous full cell with the internal integration of photoelectrode is designed for demonstrating the feasibility of the photoassisted charge strategy. The photoassisted rechargeable sodium polysulfide/iodine battery has been assembled by employing Na_2S_4 and NaI as the anolyte and catholyte respectively, and a TiO_2 photoelectrode is integrated into the catholyte for realizing the photoelectric conversion. Due to the compensation of photovoltage, this photoassisted battery can be charged with an ultralow charging voltage of 0.08 V, which is lower than its discharging voltage of 0.83 V. The charging voltage reduction translates to saving ~90% input electric energy.

For obtaining a high-voltage photoassisted rechargeable battery, the feasibility of photoassisted charge strategy in an organic rechargeable battery has been investigated, simultaneously the feasibility of visible light-driven photoelectrode in organic battery has been demonstrated. The designed photoassisted rechargeable battery employs the P2-$Na_{0.66}Ni_{0.17}Co_{0.17}Ti_{0.66}O_2$ and NaI as the active materials of anode and cathode, and

a Ta_3N_5 as a visible light-driven photoelectrode is inserted into catholyte for harvesting the solar energy. Under the visible light, a low charging voltage of 1.65 V is achieved, which is lower than its discharging voltage of 2.02 V. The charging voltage reduction results in the ~14% input electric energy saving.

The conventional organic/aqueous hybrid batteries combine the advantages of organic batteries and aqueous batteries with the high voltage window and fast transfer for several ions. Thus, a photoassisted rechargeable hybrid lithium-ion battery for photoassisted charging has been assembled with using the metal Li and $LiFePO_4$ respectively as anode and cathode, and a TiO_2 photoelectrode is inserted into catholyte for capturing the solar energy. Under the illumination, the photoassisted chargeable lithium-ion battery can be charged at a voltage of 2.78 V, which is lower than its discharging voltage of 3.41 V. The charging voltage reduction results in input energy saving of ~20% compared to conventional lithium-ion battery.

Through designing three-types photoassisted rechargeable batteries with the internal integration of simplified photoelectrode, the feasibility and performance of solar-energy conversion/storage in rechargeable batteries have been evaluated. Our strategy and designed systems provide a significant direction for the large-scale energy applications of solar energy.

TABLE OF CONTENTS

LIST OF FIGURES

LIST OF TABLES

Chapter 1. General Introduction

1.1 Urgent demand for solar energy conversion and storage

With the increasing energy requirement and environmental hazard, development and application of renewable energy have become a matter of great urgency. Solar energy, one of most promising renewable energy, possesses the abundant storage about 23000 TW year^{-1} and can completely meet the world energy consumption around 16 TW year^{-1}) as shown in Fig. 1.1.[1, 2] Meanwhile, the low-costs and nonpolluting source endow solar energy with huge prospect of the practical applications. However, the inherent intermittency of solar energy hinders its widespread utilizations, and this shortcoming simultaneously plagues other kinds of renewable energy. Consequently, the development for solar energy conversion/storage systems has become extremely significant to balance the various requirements of devices and consumption.

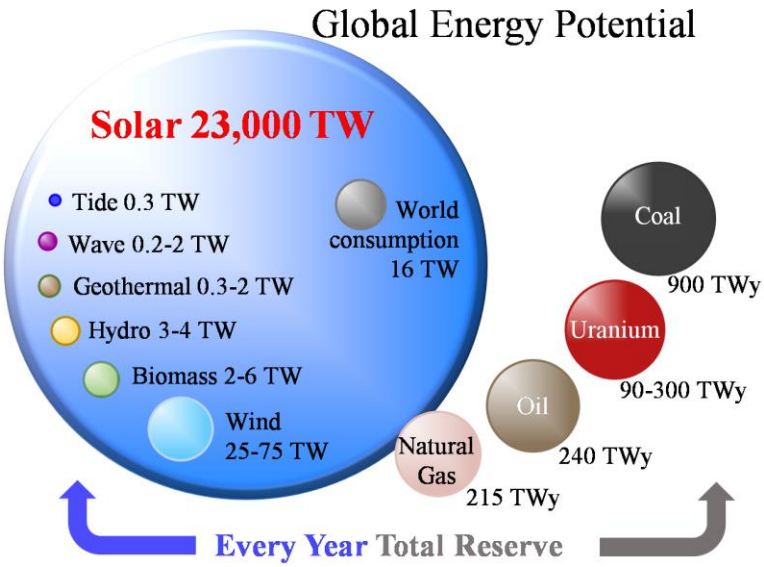

Fig. 1.1 Global energy potential and world consumption/every year (Wikimedia commoms).

Therefore, photocharging energy storage devices have been widely concerned by a lot of researchers. Because these systems can realize the conversion and storage of free and abundant solar energy into the electric energy with saving the input electric energy, meanwhile can output the electric energy which is similar with the conventional devices. However, up to date, the photocharging energy storage devices have mainly focused on the integration of photovoltaic cells and battery into one device, which exhibited a high cost and very low photoelectric conversion and storage efficiency. Thus, the internal integration of a photoelectrode into the device by a photoassisted charging strategy is considered as an ideal future solution for achieving the high-effective conversion and storage of solar energy.

1.1.1 Conventional applications of solar energy

The solar energy can be captured by the photocatalysts. Therefore, before developing the applications of solar energy into rechargeable batteries, it is necessary to deeply understand the characteristics and conventional applications of photocatalysts. The photocatalyst is a catalyst applied in the photocatalysis for promoting the photochemical reaction. In accordance with the phase types of photocatalysts and reactants in photocatalysis, the photocatalysts can be categorized into two types: homogeneous photocatalysts and heterogeneous photocatalysts.[3-5] In homogeneous photocatalysis, the reactants and photocatalysts exist in the same phase, and the common homogeneous photocatalysts include the photo-Fenton and ozone systems. Oppositely, in heterogeneous photocatalysis, the catalysts have the different phase with the reactants, and the common photocatalysts mainly involve the transition metal oxides and semiconductors. The semiconductor-photocatalysts owning the inconsecutive energy bands display the ‘photo-excited state’ feature under the

illumination. After absorbing the light irradiation, the electrons (e^-) in the valence band (VB) of photocatalyst are excited and migrate to the conduction band (CB), while the holes (h^+) are left in the VB as shown in Fig. 1.2a.

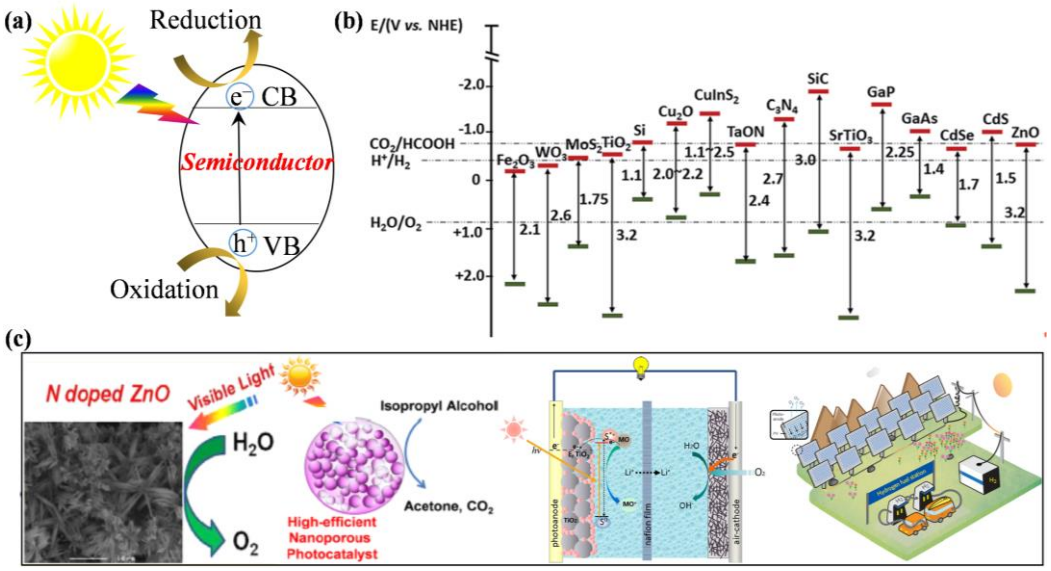

Fig. 1.2 (a) Working mechanism of semiconductor photocatalysts. (b) Conduction band (red line) and valence band (green line) positions of the reported photocatalysts (V vs. NHE, pH=7).[6] Copyright 2014 Royal Society of Chemistry. (c) Conventional applications of solar energy.[8-11] Copyright 2013 American Chemical Society. Copyright 2014 American Chemical Society. Copyright 2016 Elsevier. Copyright 2017 Nature Publishing Group.

The band gap of semiconductor between the bottom of CB to top of VB, decides the absorbed region of solar spectrum. For example, the visible-light accounts for more than 40% of sunlight, and its spectrum ranges from 400 nm (3.12 eV) to 800 nm (1.56 eV). In Fig. 1.2b, the GaP, Fe_2O_3 and C_3N_4 are all the typical visible-light driven

photocatalysts.[6] The photocatalytic activity mainly depends on the ability of the catalyst to generate e^--h^+ pairs. Since the reduced the particle size is generally beneficial for surface-dependent photocatalysis, nanophotocatalysts have been widely investigated in the practical applications. Inspired by the significant finding on TiO_2 photocatalysis by Honda-Fujishima effect in 1967,[7] various nanophotocatalysts have been exploited and utilized for solving the contemporary issues such as photocatalytic water splitting, organic contaminant decomposition, energy harvesting devices and decomposition of crude oil and so on (Fig. 1.2c).[8-11] The following section reviews the recent progress on the above-mentioned applications.

Firstly, the application of solar energy in photocatalytic water splitting. The water splitting includes the two kinds of reactions: OER (oxygen evolution reaction) and HER (hydrogen evolution reaction). However, the achievement of an efficient OER is significantly more challenging than that of HER, because of the OER involves multiple electron transfer and thereby suffer from sluggish kinetics. For developing on the photocatalytic water splitting, the use of earth-abundant elements for preparing the low-cost photocatalysts and the acquisition for the high-activity photocatalysts are two main researched directions. The various nanophotocatalysts with controlled morphologies has been reviewed and discussed by Tong et al. The author has compared the different materials including the distinctions of including one-dimensional nanostructures, facet-controlled semiconductor materials and hierarchical composite nanostructures, and highlighted the significance of high quantum yield (QY).[12] In the case of pure water photocatalytic splitting, the highest QY thus far is 56%, reported for La-doped $NaTaO_3$ under UV irradiation (λ = 270 nm).[13] Besides, an extremely high QY of nearly 90% under visible light (λ = 420 nm) was found using Ag_3PO_4 for the evolution of O_2 in water photolysis.[14] Luo et al. detailedly summarized the advantages of 2D nanoscale-materials in photocatalytic

areas and highlighted heterojunction architectures based on interfacial engineering at the nanoscale and energy diagram alignment of 2D material, which are expected to further facilitate charge separation and transport along with enhanced photocatalytic performance.[15] Liu et al. emphatically reviewed the influence of crystal growth, doping and heterostructuring on the TiO_2-based photocatalysts with unique and properties.[16] In addition, Meng et al. summarized and demonstrated that the nanometals serving as cocatalysts, play an indispensable role in fundamentally improving the photocatalytic performance of photocatalysts.[17] In practical, the most efficient OER catalysts in acidic or alkaline solutions are noble metal-based catalysts such as IrO_2 and RuO_2, but they suffer from the disadvantages of high cost and scarcity. Therefore, it is requisite to explore photocatalysts with low-cost and high-performance, and the transition metal Mn-, Co- and Ni- based oxides and carbon nitride et al. are fortunately emerging as the potential candidates. Robinson et al. reported the nanosize λ-MnO_2 obtained from the nanocrystalline $LiMn_2O_4$, showing a significantly higher water oxidation catalytic activity (Turnover Frequency: 3×10^{-5} mol O_2/s/mol Mn) than that with micrometer and irregular particle sizes.[18] Additionally, the feasibility to activate the catalytic oxidation of water by cubic $Li_2Co_2O_4$ also has been demonstrated by Gardner et al. In contrast, polymorph $LiCoO_2$ can hardly catalyze the water splitter reaction.[19] Gong et al. presented that the ultrathin NiFe-LDH nanoplates incorporated on mildly oxidized multiwalled carbon nanotubes exhibited higher OER electrocatalytic activity and better stability than a commercial precious metal IrO_2 catalyst.[20] Furthermore, the low-cost carbon nitride nanosheets have showed the great potential in the photocatalytic hydrogen evolution by the visible-light-driven, such as the graphene-like carbon nitride nanosheets and vanadate quantum dots/graphitic carbon nitride nanosheets and so on.[21, 22]

Secondly, the application of solar energy in organic contaminant decomposition. The self-decomposition of organic contaminants at room temperature is kinetically slow, while the employment of the e^--h^+ pairs from motivated nanophotocatalysts is conducive to accelerate degradation ability. The typical working mechanism is shown in the following process:

$$h\nu \rightarrow \text{photocatalyst} \rightarrow e^- + h^+$$

$$\text{Org} + h^+ \rightarrow CO_2 + H_2O + \text{other products}$$

$$O_2 + 2H^+ + 2e^- \rightarrow H_2O_2$$

On the illumination, the excited h^+ from photocatalysts can oxidize surface absorbed H_2O to form •OH radicals which could attack organic contaminants or directly oxidize organic molecules. At the same time, the excited e^- can react with O_2 to yield superoxide radical anions $\bullet O_2^-$ species. For example, Ouyang et al. fabricated a nanoporous $SrTiO_3$ photocatalyst by a nanotemplate assisted sol−gel hydrothermal technique, and this particular nanoporous attained a great enhancement in photocatalytic efficiency by eliminating isopropyl alcohol (IPA) degradation into acetone and CO_2.[9] Ag_3PO_4 photocatalyst shows larger quantum yields compared with the well-known oxidation photocatalysts such as TiO_2, $BiVO_4$, and WO_3, and Martin et al. concluded the organic decomposition of Ag_3PO_4-based nanophotocatalysts and suggested that the faceted crystals induced high activity due to preferential charge transfer to specific crystal planes.[23] Note that the surface plasmon resonance effect of Ag nanoparticle in this type nanophotocatalysts is still a vital issue needed to be further improved.

Thirdly, the application of solar energy in energy harvesting devices. Profit from the superiority on the water splitting and decomposition, nanophotocatalysts could be applied in the fuel cells for sustainable and clean electricity generation. Cui et al. used TiO_2 nanoparticles as photoanode and constructed a solar storable fuel cell with

efficient photo-degradation of organic contaminants in waste water for direct electricity generation and this cell delivered a stable voltage of ~0.6 V at a constant current of ~20 μA cm^{-2}, resulting in almost complete degradation of methyl orange (MO) in aqueous solution in 1 h.[10] Moreover, the common photovoltaic cell is a kind of electrical device that directly converts the solar energy into electricity by the photovoltaic effect, and the plenty of nanophotocatalysts have been widely used in photovoltaic cells (PVs), such as the Si-based solar cells, perovskite solar cells (PSCs) and dye sensitized solar cells (DSSCs). In particular, the low-cost, high-efficiency PSCs and DSSCs have shown appealing potential in practical applications.[24-28] Landman et al. constructed the photoelectrochemical-photovoltaic tandem cells connected by metal wires to a centralized H_2 generator at the refuelling station.[11] This separated cell delivered a high solar-to-hydrogen conversion efficiency of 7.5%, which can readily surpass 10% using standard commercial components.

Finally, the other applications of solar energy. Nanophotocatalysts have been extensively investigated in the areas of photoelectrochemical reduction of carbon dioxide, decomposition of crude oil and so on. Zhao et al. have taken a prospective review on the nanosemiconductor/metal complex co-catalyst for converting carbon dioxide (CO_2) into more valuable chemicals, and pointed out the pairing the suitable semiconductors with these metal complexes was promising for methanol or methane production hybrid catalysts.[6] Zhao et al. applied TiO_2 photocatalysts to destruct volatile organic compounds in indoor air, and emphatically studied the dependence of reaction rate on some key factors (moisture, light intensity and initial contaminant concentration).[29] TiO_2 and ZnO nanoparticles have also been adopted for the photocatalytic degradation of diesel oil and crude oil.[30, 31] And this process has become an innovative idea that can be implemented in future environmental usage.

In a short summary, a brief introduction for the conventional applications of solar

energy has been taken for providing a comprehensive understanding and offer a valuable reference for the solar energy storage in rechargeable battery.[32, 33] Although, there are still some challenges on the further exploitation for photocatalysts, these excellent researches on the photocatalysis in aqueous, organic and gas substances offer a valuable reference for the solar energy storage in other fields.

1.1.2 Rechargeable batteries have great potential for solar energy storage

The common photovoltaic cells (PVs) only covert solar energy into electric energy for the straight usage to energy clients, without the enduringly stored function (Fig. 1.3a). Therefore, the exploration for the simultaneous conversion and storage of solar energy is seriously urgent. Among numerous energy storage devices, the rechargeable batteries enable to covert electric energy into the storable chemical energy and realize the recyclable conversion/storage between electric energy and chemical energy (Fig. 1.3b) and are considered as a promising generation due to the high specific energy and power, long cycle life and so on.

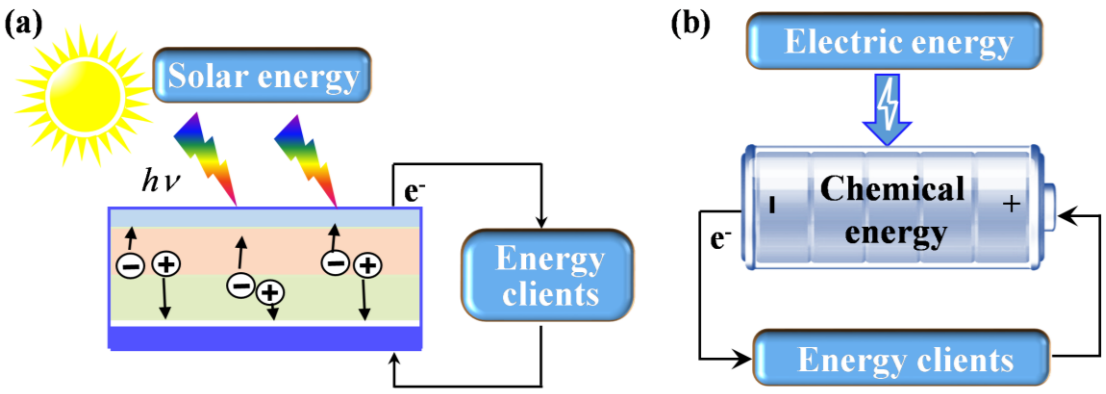

Fig. 1.3 Typical characteristics of photovoltaic cells (a) and rechargeable batteries (b).

In addition, the rechargeable batteries have been developed as the one of most efficient systems for the electrical energy storage, which are extensively used in modern society due to the increasing electric requirements and have been widely applied into the various fields such as portable electronic equipment, electrical vehicles, aerospace and other important areas. Different from the PVs with the only conversion function, the rechargeable batteries are based on the energy conversion and storage between electrical energy and chemical energy. Harvesting solar energy into high-performance rechargeable batteries could not only achieve the large-scale utilizations of solar energy, but also short the path from renewable energy to electric energy. The highly effective, long-durable, less-expensive and environmentally-friendly incorporation of solar energy into batteries are the key to challenge, and substantial research efforts have been devoted to this popular direction.

1.2 Rechargeable batteries

1.2.1 Brief introduction of rechargeable batteries

A rechargeable battery, also called as secondary cell is a type of electrical battery which can be charged from input electric and discharged to energy clients, and recharged many times.[34] It is mainly composed of anode, separator, electrolyte and cathode. Based on the different electrolyte, the systems of rechargeable batteries can be segmented into the organic, aqueous, organic/aqueous hybrid and solid systems. While, due to the limit of some issues in solid electrolyte such as polarization, the organic, aqueous, organic/aqueous three systems have been extensively applied in many commercial products, and the fabrication of three systems are shown in Fig. 1.4. Rechargeable batteries have been produced in many different shapes and sizes,

ranging from button cells to megawatt systems connected to stabilize an electrical distribution network. Several different combinations of electrode materials and electrolytes are used, including lead–acid, nickel cadmium (NiCd), nickel metal hydride (NiMH), lithium-ion (Li-ion), and sodium ion (Na-ion) batteries (Fig. 1.5).

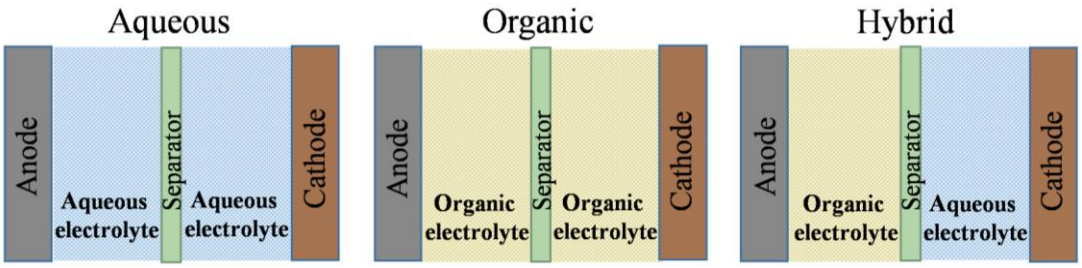

Fig. 1.4 Three typical architectures of conventional rechargeable battery.

The lead–acid battery, invented by Gaston Planté et al. in 1859, is the oldest and first practical rechargeable battery.[35] Although the energy-to-volume ratio and low energy-to-weight ratio are very low, its ability of supplying high surge currents exhibits that the cells have a relatively high power-to-weight ratio. Especially, the low-cost feature makes it attractive for utilizing in motor vehicles to provide the high current required by automobile starter motors. In 1899, The Ni-Cd battery employing the nickel oxide hydroxide and metallic Cd as electrodes was proposed by Waldemar Jungner et al..[36] Cd is a toxic element, and prohibited for most uses by the European Union in 2004. Ni-Cd batteries have been almost completely replaced by nickel–metal hydride (NiMH) batteries, and the NiMH became available in 1989.[37, 38] These are now a common consumer and industrial type. The battery has a hydrogen-absorbing alloy for the negative electrode instead of cadmium. The lithium-ion battery was introduced in the market in 1991, and it is the choice in most

consumer electronics and has the high energy density and a very slow loss of charge when not in use.[39-41] The increasing cost and limited availability of lithium suggest that an alternative to lithium-ion batteries should be developed to meet the large-scale requirements. sodium-ion batteries have a similar chemical storage mechanism as their lithium-ion counterparts, and are expected to be low cost and chemically sustainable owing to an almost infinite supply of sodium.[42, 43] Currently the reported rechargeable batteries with high energy density are shown in Fig. 1.5.

Fig. 1.5 Reported rechargeable batteries with high energy density (Wikipedia and google).

1.2.2 Operation mechanism of rechargeable batteries

From rechargeable batteries, the typical operation mechanism is presented in Fig. 1.6. During the charging process, an input electric energy is conducted on the anode and cathode, and the cathode materials are oxidized to their oxidation form (C^{ox}) with releasing cations, while the electrons are transported from the cathode to the anode through an external circuit. The anode materials are reduced to their reduced form (A^{red}). During the discharging process, the evolutions of anode and cathode are reversible. In this process, an extra electric energy is needed to realize the conversion

of electric energy to chemical energy. In order to save the extra electric energy during the charging process, more recent efforts have been focused on ways to utilize solar energy to power rechargeable batteries.

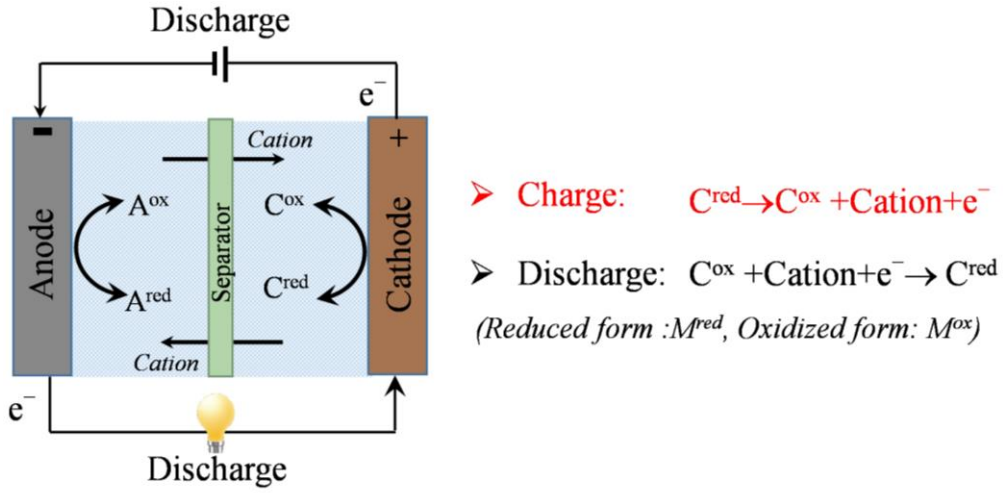

Fig. 1.6 Charge/discharge mechanism of rechargeable battery.

1.3 Strategies of solar energy conversion and storage in rechargeable batteries

1.3.1 External combination of PVs in rechargeable batteries

The photovoltaic cells (PVs) have been well-known as one kind of the fastest growing renewable energy technologies. However, the intermittency of PVs output power has been a major shortcoming owing to its direct coupling to the availability of the solar irradiance. Rechargeable batteries have the merits of enabling the continuous and long-term charge/discharge, especially for some commercialized Li-ion batteries. Therefore, attempts to power electric energy using two independent energy harvesting

and storing devices have already been pursued for the large-scale practical applications of solar energy as shown in Fig. 1.7a.

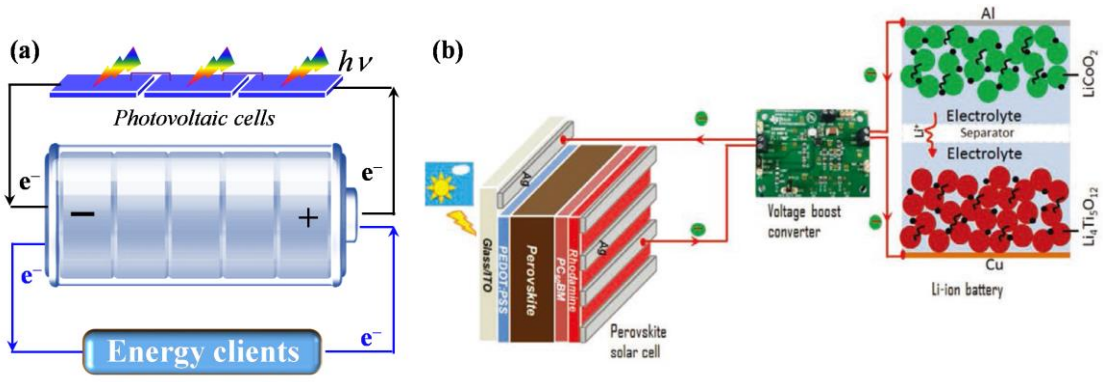

Fig. 1.7 (a) External photovoltaic cells into rechargeable batteries. (b) Reported photocharging plots of $Li_4Ti_5O_{12}$-$LiCoO_2$ cell using by DC-DC booster.[44] Copyright 2017 Wiley-VCH Verlag GmbH.

The common PV is a kind of electrical device that directly converts the solar energy into electricity by the photovoltaic effect, and the plenty of nanophotocatalysts have been widely applied in photovoltaic cells (PVs), such as the dye sensitized solar cells (DSSCs), perovskite solar cells (PSCs) and Si-based solar cells. Especially, the low-cost, high-efficiency PSCs and DSSCs have shown appealing potential in practical applications.[24-28] Based on the excellent performance of PVs, a solar photovoltaic (PV) charging of Li-ion battery has been investigated by Gibson et al. with externally wiring the high-effective silicon PV modules into the iron phosphate type Li-ion cell.[45] The assembled system could be charged at a rate of up to 1.5 C with an average voltage of 3.37 V (full charge in about 40 min) and the optimized solar charging system efficiency reached 14.5%, by combining a 15% PV system solar to

electrical efficiency and a nearly 100% electrical to battery charge efficiency. It is noteworthy that as battery voltage passing the PV maximum power point, the rapid drop of power could significantly reduce the risk of thermal damage to battery systems during charging. Xu et al. demonstrated the use of perovskite solar cell packs with four single $CH_3NH_3PbI_3$ based solar cells connected in series for direct photo-charging lithium-ion batteries assembled with a $Li_4Ti_5O_{12}$ anode and a $LiFePO_4$ cathode. The photo-electric conversion and storage efficiency is about 7.36% at 0.5 C, moreover the discharging capacity decreased from 141 mAh g^{-1} to 111.6 mAh g^{-1} after 10 cycles.[46] In order to further enhance photo-electric conversion and storage efficiency, Gurung et al. firstly introduced an ultralow power direct current-direct current (DC–DC) boost converter into the perovskite solar cells (PSC) for photocharging a $Li_4Ti_5O_{12}$-$LiCoO_2$ battery (Fig. 1.7b).[44] This approach leads to a average storage efficiency of 77.2% and high overall efficiency of 9.36% at 0.5 C. In addition, the discharging capacity undergoes a degradation from 151.3 mAh g^{-1} to 134.4 mAh g^{-1} after 10 cycles.

Although these externally combined strategies have realized feasible conversion/storage of solar energy in rechargeable batteries and demonstrated the considerable photo-electric conversion and storage efficiency, there are still some challenges in these systems for the practical applications. For example, compared with the single rechargeable battery, the extra PVs modules and external wires increase the cost of energy storage, and enlarge the volume and weight of the entire device. In addition, the out-put electric performance of rechargeable batteries in above systems not only depends on the itself conversion, but also relies on the behaviors of PVs. Therefore, the entire systems are inflexible and solve the double problems from two single devises. Therefore, the internal integration of photoelectrodes into rechargeable batteries as one of potential solutions, has aroused the wide concerns.

1.3.2 Internal integration of photoelectrodes in rechargeable batteries

A reliable and promising strategy is the internal integration of photoelectrodes into rechargeable batteries. As shown in Fig. 1.8a, the solar-powered rechargeable battery can simplify the storage process of solar energy in the form of electricity. In this battery, the solar energy can be stored directly inside devices, and will be one of most practical systems for converting the solar energy into chemical/electrical energy. The conventional rechargeable batteries mainly consist of the anode, cathode, separator and electrolyte and can be divided into the organic, aqueous and organic/aqueous systems based on different electrolytes. In addition, considering the various types of the usable active materials, the electrodes of rechargeable batteries involve the solid, gas and liquid three types. Thus, the internal integration of photoelectrodes into rechargeable batteries will need the highly compatible coordination based on the potential energy of each part for importing the high-effective electric energy (Fig. 1.8b). Although, in 1976, Hodes et al. has proposed the first photo-rechargeable battery and Kanbara et al. has also investigated a photo-reaction on a semiconductor silicon/silicon oxide (P-I $\alpha Si/SiO_x$) electrode using silver iodide tungstanate ($Ag_6I_4WO_4$) in 1990.[47, 48] However, stringent issues including the nanophotocatalyst compatibility, device complexity and conversion efficiency inferiority, all together slow down the development of solar-powered rechargeable batteries. Until recently, the increasing studies and reports have focused on the direct integration of photoelectrodes into the rechargeable batteries from two sections including employing the seminar photoelectrodes and photoelectrodes from apart of PVs.

Firstly, the internal integration of seminar photoelectrodes in rechargeable batteries. The semiconductor-photocatalysts with inconsecutive energy bands have the typical ‘photo-excited state’ feature. Under the light irradiation, the electrons (e^-) in the valence

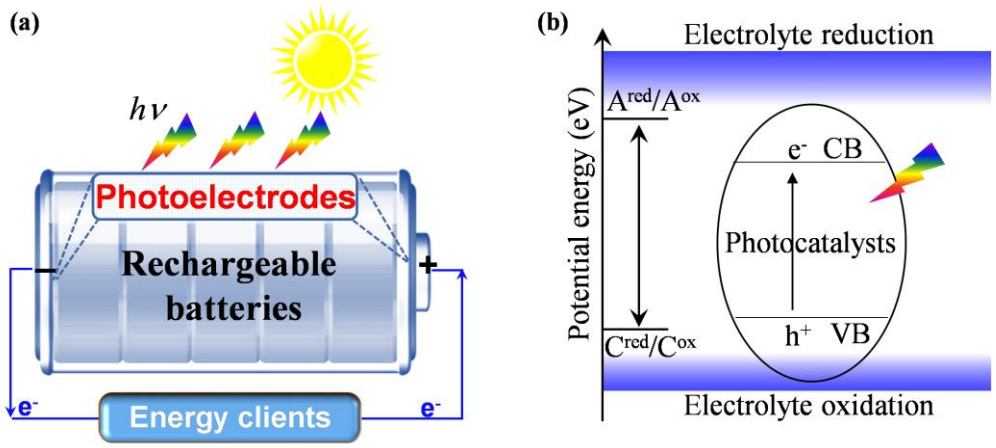

Fig. 1.8 (a) Schematic diagram of internal integration photoelectrodes into the rechargeable batteries. (b) Potential energy of the considerable three sections including the anode and cathode of rechargeable batteries, CB and VB of photocatalysts, and reduction and oxidation of electrolyte. (reduced form: M^{red}, oxidized form: M^{ox}, CB: conduction band and VB: valance band).

band of the photocatalyst are excited to the CB (conduction band), while the h^+ (holes) are left in the VB (valence band). The band gap between the top of VB to the bottom of CB, is responsible for the absorbed region of solar spectrum. The photocatalytic activity mainly depends on the ability of the catalyst to generate e^--h^+ pairs. Motivated by the significant finding on TiO_2 photocatalysis by Honda-Fujishima effect in 1967,[7] various works have been reported with the generation of H_2 or O_2. Among various electrochemical energy storage devices, Li-sulfur (Li-S) batteries hold great promise because sulfur is environmentally friendly and naturally resourceful and possess a high gravimetric theoretical capacity of 1672 mAh g^{-1}.[49-56] Sulfur undergoes a series of structural changes as described by the redox reaction of S_8 + 16 Li ↔ $8Li_2S$ (~2.15 V

vs. Li/Li^+) during the discharging and charging processes.[56] In 2015, Li et al. reported the direct capture and storage of solar energy into the aqueous Li-S battery with the configuration of Li/organic electrolyte/Li_2S_n catholyte integrated by Pt/CdS photocatalyst.[57] The absorbed solar energy was used to oxidize S^{2-} ions to polysulfide ions, thus the charge process is achieved by photo-charging process without any electrical input. After 2 h light irradiation, the solar Li-S battery exhibited a capacity of 792 mAh g^{-1}. Furthermore, with 10 min photo-charging, a specific capacity of 201 mAh g^{-1} could be achieved, which was comparable to that of Li-ion battery currently available. The good stability of solar Li-S battery was demonstrated by the high capacity retention of 92.5% after 10 cycles. Moreover, this device could also be operated under natural sunlight irradiation. The battery delivered a specific capacity of 280 mAh g^{-1} under 2 h sunlight irradiation, implying its feasible application on future large-scale storage of solar energy. Although, this system has achieved the prominent electrochemical storage of solar energy, the chemical fuel conversion of solar energy also exists. Thus, the solar energy storage in the closed Li-S battery will be an important research direction in the future. Lou et al. demonstrated the feasibility of nanocrystalline MoO_3 as photocatalyst and intercalation host materials for high energy density Li-ion batteries under the illumination, the photocharging mechanism was as shown in the following process: $MoO_3 + h\nu \rightarrow MoO_3^* + e^- + h^+$, $4h^+ + H_2O \rightarrow 4H^+ + O_2$, $MoO_3 + xA^+ + xe^- \rightarrow A_xMoO_3$.[58] Kim et al. designed an environmental friendly, namely- "solar water battery", based on a water oxidation reaction instead of the redox chemistry of a catholyte and the assembled battery could discharge at a stable voltage plateau of ~0.6 V. Although the specific discharge capacitance of the battery was not so high (~10 mAh g^{-1} after 16 h of photocharging), there is considerable scope for improvement by adapting the numerous materials and technologies.[59] Thimmappa et al. proposed a more simplified device using TiN as photoanode in a system (Fig.

10b).[60] The battery could charge at a high discharge voltage of ~0.8 V after the self-photocharging, especially it could work using ambient light with the great potential applied in the presence of street light, household lighting, indoor lighting, and so on. While in above systems, the photo-generated hydrogen or oxygen need to be initially stored in the external equipment.

Secondly, based on the enlightenment of PVs, the increasing studies and reports have focused on the internal integration of photoelectrodes from PVs in various rechargeable batteries. For instance, Guo et al. reported a new integrated power pack consisting of a DSSC and a LIB is fabricated based on double-sided TiO_2 nanotubes anode.[61] When sun light irradiates on the DSSCs, the excited electrons induces the following chemical process as $TiO_2 + xLi^+ + xe^- \rightarrow LixTiO_2$ on the TiO_2 anode, simultaneously the reaction of the cathode ($LiCoO_2 \rightarrow Li_{1-x}CoO_2 + xLi^+ + xe^-$) releases free electrons that flow to the Pt electrode by an external circuit for combining with the excited holes. By using this hybrid structure, the system delivers a discharge capacity of ~38.89 μAh under the discharge density of 100 μA with the voltage charged to ~3 V in ~8 min, and a total of 0.82% energy conversion and storage efficiency has been achieved. Paolella et al. introduced a simpler two-electrode system involving direct photo-oxidation of $LiFePO_4$ nanocrystals by light irradiation in the presence of the N719 dye as hybrid photo-cathode and Li metal as anode.[62] This system showed a relatively fast photo-assisted OCV (<24 h) and a high capacity that is at least two times the theoretical one. However, it is regretful that the voltage plateau decreases below the 3.4 V from the 5^{th} cycle. The nonaqueous Li-O_2 battery shows appealing potential for large scale solar energy storage due to the paramount theoretical energy density (~3550 Wh kg^{-1}), which is several times higher than that of conventional Li-ion batteries (~387 Wh kg^{-1}).[63-68] This is because lithium metal as the anode and oxygen gas as the cathode can be absorbed freely from the ambient air,

thus greatly reduce the weight of Li-O_2 battery. The use of inexhaustible oxygen gas as the cathode material is a strong advantage for its future development as well. Typically, a Li-O_2 battery is composed of a porous carbon cathode, a lithium metal anode and a Li^+ ion conductive electrolyte. In this battery, the fundamental electrochemical reaction is: $2Li^+ + 2e^- + O_2 \leftrightarrow Li_2O_2$, which relies on the reversible formation and decomposition of Li_2O_2 upon cycling with an equilibrium voltage of 2.96 V vs. Li/Li^+.[69] Therefore, the integration of solar energy with Li-O_2 battery offers an inspirational strategy for simultaneous conversion and storage of solar energy. Meanwhile, by absorbing solar energy, the pressing challenge of large charge overpotential in Li-O_2 batteries can be effectively addressed. Wu et al. initially proposed a photoassisted rechargeable device by integrating a TiO_2-dye photoelectrode into a Li-O_2 battery.[70] During the charge process, the TiO_2 photoelectrode could drive the oxidation of discharge product (Li_2O_2), thus capturing solar energy and storing it as electrochemical energy. Due to the utilization of solar energy, the Li-O_2 battery to be charged at an input voltage of 2.8 V, which was much lower than that of a conventional Li-O_2 battery (~4.0 V) and the battery can be discharged similar with the conventional battery. In order to attain the higher energy density (>250 Wh g^{-1}) and high power density with the rapid charge and discharge rates, Li-iodine (Li-I) batteries owning the more-positive potential of I_3^-/I^- (~3.5 V versus Li^+/Li) and high theoretical capacity (211mAhg^{-1}), have been considered as the next-generation lithium-ion batteries for the long-range electric vehicles and large-scale energy storage.[71-73] Particularly, an aqueous I_3^-/I^-catholyte possessing the high solubility has been in the flow-through-mode system for the prominent performance.[74, 75] Meanwhile, this aqueous catholyte is favorable to the direct linkage with the photoelectrode for high-effectively converting and storing the solar energy. Yu et al. demonstrated the photoassisted charging concept for a solar-powered Li–I flow battery by incorporation

of a dye sensitized TiO_2 photoelectrode into a Li–I redox flow battery.[76] The most remarkable feature is that the guanidine thiocyanate (GuSCN) and chenodeoxycholic acid (Cheno) additives effectively facilitate the surface-wetting between the hydrophilic I_3^-/I^- electrolyte and the hydrophobic dye sensitized. This the Li–I SFB deiveres a fast light-response and a stable charging voltage plateau at 2.9 V remained for 25 cycles, thus demonstrating energy savings up to 20% for conventional Li-I batteries. The relative works on the internal integration of photoelectrodes have been summarized in the Table 1.

Table 1. Reported works about the internal integration of photoelectrodes in various rechargeable batteries.

Type	Photo electrode	Active material in anode/cathode	Separator	Discharge voltage	Capacity	Tested cycling numbers	η_1	η_2	Ref.
Li-ion batteries	Dye sensitized electrode	$TiO_2/LiCoO_2$	PE	~ 2 V	38.89 μA	3 cycles (>100% capacity retention)	0.82%	-	[61]
	N719 dye/$LiFePO_4$	Li/$LiFePO_4$	-	~3.4 V	340 mAh g^{-1}	15 cycles (~100% capacity retention)	0.06-0.08%	-	[62]
Li-O_2 batteries	Dye sensitized electrode	Li/O_2	Glassy fiber	~2.8 V	-	4 cycles (2.72 V→~3.10 V)*	-	~103%	[70]
Li-S batteries	CdS/Pt	Li/S	LISICON	2.53 V	792 mAh g^{-1}	10 cycles (92.5% capacity retention)	-	-	[57]
Li-I batteries	Dye sensitized electrode	Li/I	LISICON	3.3 V	32600 mAh L^{-1}	25 cycles (2.91 → 2.93 V)*	-	120%	[76]
Redox or redox-flow batteries	Dual-silicon	AQDS/HBr	Nafion 115	0.78 V	730 mAh L^{-1}	10 cycles (~98% capacity retention)	~3.2%	-	[77]
	Silicon solar cells	AQDS/BQDS	Nafion 212	~0.41 V	3500 mAh L^{-1}	10 cycles (~91% current retention)	1.7%	-	[78]
	Dye sensitized electrode	Li_2WO_4/LiI	LISICON	~0.5 V	0.0195 mAh mL^{-1}	10 cycles (98.6% capacity retention)	-	-	[79]
	Dye sensitized electrode	AB5-type hydrogen storage alloy/LiI	Modified Nafion 117	~0.6 V	26.7 mAh g^{-1}	20 cycles (~88% capacity retention)	<1%	-	[80]
other batteries	TiO_2	WO_3/H_2O	LICGC	0.6 V	10 mAh g^{-1}	10 cycles (85% capacity retention)	-	-	[59]
	TiN	$KFe[Fe(CN)_6]/H_2O$	-	~0.8 V	77.8 mAh g^{-1}	100 cycles (97.9% capacity retention)	-	69.5%	[60]

*η_1: photoelectric conversion and storage efficiency, η_2: electric energy efficiency. *: photoassisted charging voltage.*

In above reports, a photoassisted charging strategy has gradually emerged because of its effective output power and avoiding the generation of other extra products such as H_2 and O_2. However, the integrated photoelectrodes from PVs doubtlessly increase the cost and complex of whole system. Therefore, the development of simplified and effective photoassisted rechargeable battery is a great challenge.

1.4 Target and outline of this dissertation

1.4.1 Motivation of this research

Rechargeable batteries have shown the great potential of enabling the continuous and long-term charge/discharge. Therefore, the internal integration of simplified photoelectrode into rechargeable batteries will be expected for the high-effective solar conversion/storage and help rechargeable batteries save much input-electric energy. The photoassisted rechargeable batteries could be designed as shown in the Fig. 1.9. After the photoassisted charging, the battery could discharge similar with that of conventional rechargeable batteries and will deliver the closed capacity. Because the photocatalysts have been employed in photocatalytic water splitting and aqueous solutions have the good conductivity and fast diffusion-rate of ions, a photoassisted rechargeable aqueous battery is noteworthy designed for the high-effective performance. While the aqueous batteries all have the limited voltrgae, a photoassisted rechargeable organic battery could be in virtue of the high-voltage advantage of conventional organic battery. Furthermore, the conventional organic/aqueous hybrid batteries combine the advantages of organic and aqueous batteries with the high voltage window and metal anode which has the ultralow voltage. The conversion/storage of solar energy in hybrid batteries will deliver a high voltage and fast photo-electric transformation. Therefore, attempts to assemble photoassisted

rechargeable batteries with the simplified, high-effective, low cost and eco-friendly features will promote the large-scale practical applications.

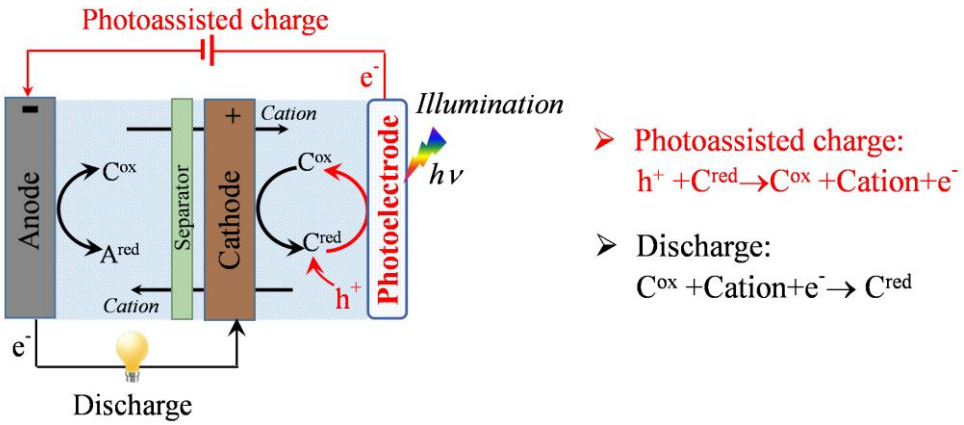

Fig. 1.9 Photoassisted rechargeable mechanism of designed battery under illumination.

1.4.2 Targets of this research

The targets of this research on the conversion/storage of solar energy into conventional rechargeable batteries are as follows:

To realize the conversion and storage of solar energy in rechargeable aqueous battery by designing a photoassisted rechargeable aqueous battery (Fig. 1.10 a).

To achieve a high output-voltage by assembling a photoassisted rechargeable organic battery (Fig. 1.10 b).

To get a fast light-response and high output-voltage by assembling a photoassisted rechargeable hybrid battery (Fig. 1.10 b).

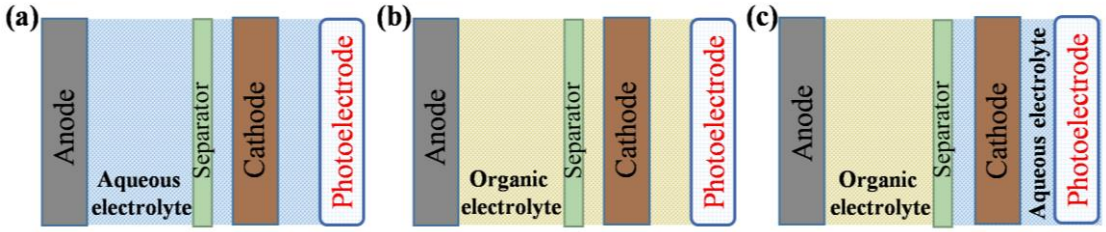

Fig. 1.10 Solar energy storage in three-types batteries including photoassisted rechargeable aqueous battery (a), photoassisted rechargeable organic battery (b) and photoassisted rechargeable hybrid battery (c).

1.4.3 Outline of this thesis

This dissertation consists of the following five chapters:

Charter 1 is the general introduction for the whole work. It mainly includes the background of solar energy conversion and storage, rechargeable batteries, strategies of solar energy conversion and storage in rechargeable batteries. The motivation and target of research have been proposed.

In chapter 2, Conversion and storage of solar energy in rechargeable aqueous battery has been demonstrated by designing a photoassisted rechargeable SPIB. By utilizing solar energy, the charging voltage of this battery has been reduced to 0.08 V which is even much lower than the discharging voltage (0.83 V), and this ultralow charging voltage leads to saving ~90% input electric energy.

In chapter 3, Conversion and storage of solar energy in rechargeable organic battery has been demonstrated by assembling a photoassisted rechargeable SIB battery. Under the light radiation, the charging voltage of this battery has been reduced to 1.65 V, and

~14% input electric energy has been saved due to the compensation of solar energy.

In chapter 4, Conversion and storage of solar energy in rechargeable hybrid battery has been demonstrated by assembling a photoassisted rechargeable LIB battery. a photoassisted rechargeable hybrid battery has been designed with a photoassisted rechargeable SPIB as the example. Under the illumination, this battery can be charged at a voltage of 2.78 V, which is lower than its discharging voltage of 3.41 V, and the charging voltage reduction results in saving ~20 % input electric energy.

Chapter 5 is the total conclusion and perspectives for future research in this field.

Chapter 2. A photoassisted rechargeable aqueous battery

2.1 Introduction

Due to the faster diffusion of ions or elections in aqueous than in the organic solution, a full aqueous is firstly chosen for demonstrating the feasibility of the solar energy storage in rechargeable batteries. However, up to now, the solar energy powered systems mainly focused on the combination of PVs and battery into one device, and these devices have the high cost and low photo-electric conversion and storage efficiency. Although there are some reports about the internal photoelectrodes in batteries, some systems still need to be further improved. Therefore, it is still a huge challenge for developing the low cost, environmentally friendly and high-performance solar energy conversion and storage systems.

The aqueous redox battery, as one of electrochemical storages, has shown the great advantages including the environmentally friendly, long cycling life and low-cost.[81-83] In the many aqueous redox couples, the Na_2S_4/Na_2S redox couple has the relatively low and stable potential, and the high theoretical capacity in conventional redox batteries. Besides, the NaI_3/NaI redox couple has the high potential, high reversibility, high solubility and relatively low toxicity. This redox couple has been a potential catholyte in the conventional aqueous redox batteries. TiO_2 as a n-type semiconductor, have attracted worldwide attention due to their great potential in capturing solar energy, and has been one of the high-efficiency semiconductor photoelectrodes for the practical solar energy conversion such as water photo-splitting and dye-sensitized solar cells. Consequently, it is worth looking forward to realizing a photoassisted rechargeable sodium polysulfide/iodine battery (SPIB) with the integration of a TiO_2 photoelectrode for solar energy storage.

In this work, a photoassisted chargeable sodium polysulfide/iodine battery (SPIB) is designed by using Na_2S_4 and NaI as the anolyte and catholyte respectively, and a TiO_2 photoelectrode integrated into the catholyte for the solar energy storage in aqueous system. Through the solar energy input, A ultralow charging voltage of 0.08 V has been obtained for this photoassisted rechargeable SPIB. Especially, the photoassisted charging voltage is obviously lower than the 0.83 V discharging voltage. The reduced charging voltage results in the input electric energy is saved ~90%. And the characteristics of high safe and low cost make the designed photoassisted rechargeable SPIB show the application potential in the further solar energy storage in the rechargeable electric storage systems.

2.2 Experiment and characterization

2.2.1 Preparation of anode catalyst and photoelectrode

CoS grown on brass mesh was prepared by a modified electrochemical deposition method. The prepared CoS grown on brass mesh was applied the catalyst of anode and current collector.[84] The following is the detailed method: through using reactive RF magnetron sputtering device, a Co metal film was sputtered on both sides of a brass mesh, and the thickness of this film is 150 nm. Then, an in-situ electrochemical deposition was employed for wrapping a tight CoS film on the pretreated brass mesh. The deposition was scanned anodically up to 0.2 V vs. a Pt electrode in a 0.005 M polysulfide electrolyte. The mass loading of CoS was ~2 mg cm^{-2}.

TiO_2 photoelectrode was prepared by the TiO_2 grown on Ti mesh, which is based on the previous reported method.[17] A Ti mesh was immersed in a $TiCl_4$ (99.0%, Aldrich) and HCl (37%, Wako) mixed solution. Then, through a hydrothermal treatment at 170 °C for 10 h, the initial nanorods TiO_2 was deposited on pretreated Ti

mesh. For improving the crystallinity, the subsequent calcination at 450 °C for 2 h was performed. The TiO_2 mass loading was ~3.5 mg cm^{-2}.

2.2.2 Assembly of photoassisted rechargeable aqueous battery

The system of photoassisted rechargeable aqueous SPIB mainly included the CoS/brass mesh/anolyte (Na_2S_4)/Nafion 117 membrane/catholyte (NaI)/Super P carbon/Ti mesh. The CoS grown on brass mesh and anolyte (Na_2S_4) were assembled into a glass cylinder as the anode side, and the anolytes with different concentrations were configured on basis of 1 M Na_2S_4 aqueous solution which prepared as the following description: 1 M Na_2S (Aldrich) was firstly dissolved in a 1 M NaOH (Wako) aqueous solution, and then 3 M sulfur (Wako) was slowly added into above solution. After the stirring for 1 day, the 1 M Na_2S_4 solution was achieved. The Super P carbon cathode and TiO_2 photoelectrode were stuck on the cathode side of a cylindrical quartz shell. The cathode was prepared by mixing the Super P carbon with polytetrafluoroethylene (PTFE) in a weight ratio of 8:2, and the prepared slurry was then cast on a Ti mesh with loading of ~2 mg cm^{-2}. The Nafion 117 member was purchased from Aldrich, and it is sealed on the top of both anode and cathode glass cylinders. After the assembly of the battery, the both sides of the battery was needed to be immersed respectively in 0.05 M NaOH and deionized water in anode and cathode for 24 h and finally washed to neutral for realizing the pretreatment of Nafion 117 membrane. The detailed system is shown in the Fig. 2.1.

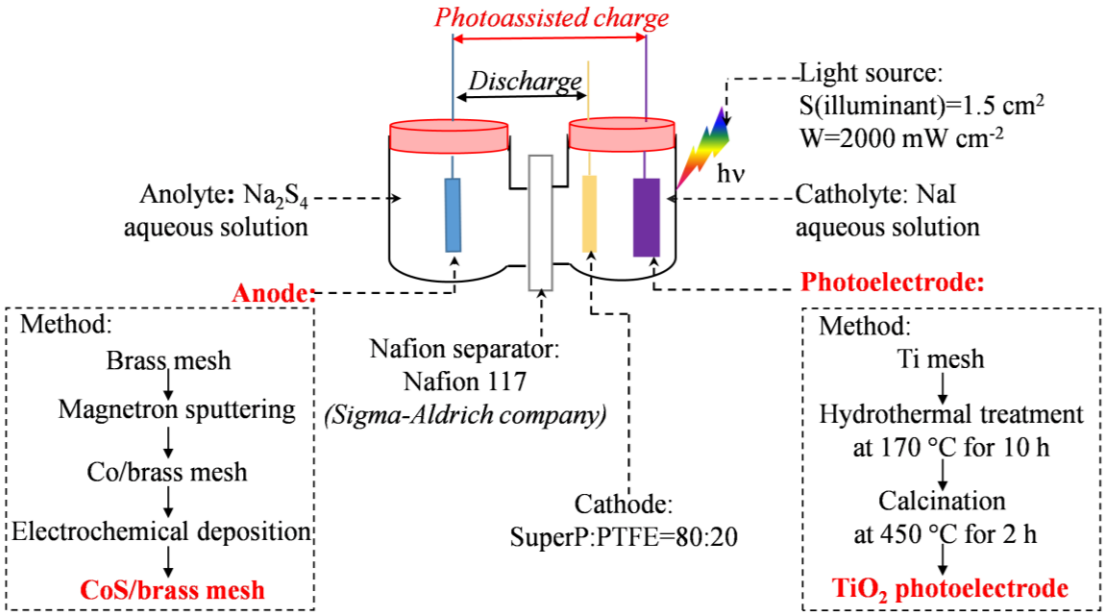

Fig. 2.1 Fabrication of a photoassisted rechargeable aqueous SPIB.

2.2.3 Electrochemical and photoelectrochemical measurements

A Solartron instrument was applied for the CV curve measurements. A Hokuto electrochemical machine was used for the charging/discharging measurements at different current densities. For photoassised charging, the photoelectrode and anode were directly connected. During the discharging process, the anode and cathode were connected. A XEF-501S Xe-lamp (San-ei Electric Co., Japan) was employed as the light source.

2.2.4 Characterizations

A Bruker D8 advanced diffractometer with Cu Kα (λ = 1.5406 Å) radiation was used for the analysis of crystal structures. A Hitachi S4800 was employed for the

SEM observation. A Shimadzu UV3101PC was used for the UV-visible absorption spectrum tests

.

2.3 Results and Discussion

2.3.1 Design of a photoassisted rechargeable aqueous battery

Fig. 2.2a shows the structure of the photoassisted chargeable SPIB, which includes S^{2-}/S_4^{2-} redox couple-based aqueous anode, I^-/I_3^- redox couple-based aqueous cathode, a Nafion 117 membrane for separating cathode and anode, and the TiO_2 photoelectrode is inserted into catholyte. On the photoassisted charging under illumination, the photoexcited holes from the valence band (VB), oxidize NaI into NaI_3 in catholyte. At the same time, the photoexcited electrons transfer from the conduction band (CB) of the TiO_2 photoelectrode into anolyte by outside circuit, resulting in the reduction of the Na_2S_4 into Na_2S. Upon the discharging, the reduction from NaI_3 to NaI and oxidation from Na_2S to Na_2S_4 are performed in the catholyte and anolyte. The discharging process are similar with the conventional SPIB. The entire process is shown in the following equations:

Photoassisted charge: $h\nu \rightarrow TiO_2 \rightarrow h^+ + e^-$ (photoelectrode)

$2h^+ + 3NaI \rightarrow NaI_3 + 2Na^+$ (catholyte)

$Na_2S_4 + 6Na^+ + 6e^- \rightarrow 4Na_2S$ (anolyte)

Discharge: $NaI_3 + 2Na^+ + 2e^- \rightarrow 3NaI$ (catholyte)

$4Na_2S \rightarrow 6Na^+ + Na_2S_4 + 6e^-$ (anolyte)

The redox potentials of S_4^{2-}/S^{2-} and I_3^-/I^- couples are respectively ~2.20 and ~3.22 V versus Na^+/Na. Therefore, the theoretical voltage of sodium polysulfide/iodine batteries is ~1 V based on above redox couples. On the basis of the potential difference between the CB value (~2.27 V versus Na^+/Na) in the semiconductor TiO_2 and redox

potential of the S_4^{2-}/S^{2-} couple, the photoassisted charging voltage of the photoassisted chargeable SPIB should theoretically be estimated to 0.07 V (2.27 - 2.20 = 0.07 V) as shown in Fig. 2.2 b.[85]. This photoassisted charging voltage is much lower than the theoretical discharging voltage (~1 V versus Na^+/Na), due to the compensation of photovoltage from the solar energy.

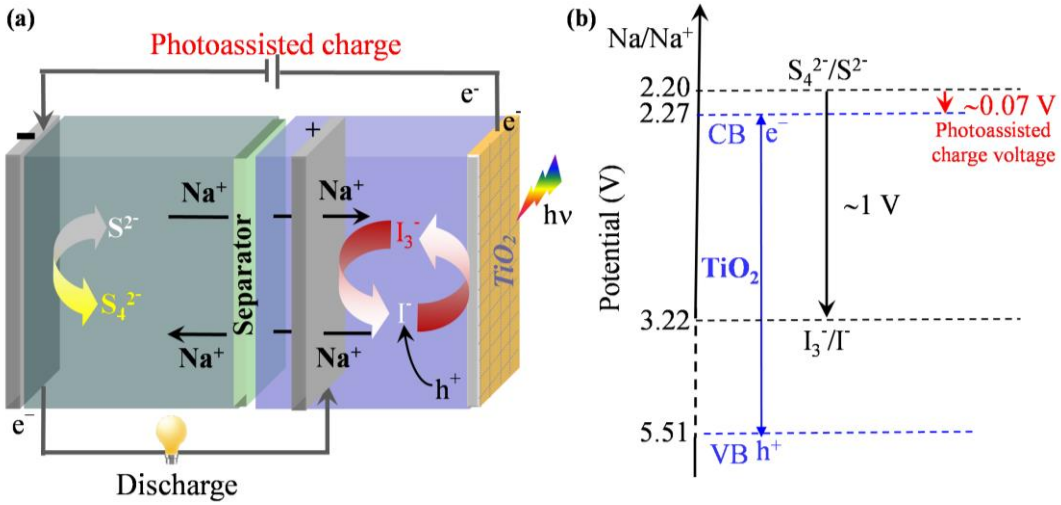

Fig. 2.2 (a) Schematic of a photoassisted rechargeable aqueous SPIB. (b) Potential diagram for the photoassisted charging process. The photoassisted charge voltage is determined by the energy difference between the anode voltage of SPIB and the quasi-Fermi level of electrons in the TiO_2 photoelectrode (near to its conduction band (CB)).

Before the photoassisted chargeable SPIB fabricated, the performance of simple SPIBs are firstly investigated. In the simple SPIB, the CoS/brass mesh and Super P/Ti mesh were respectively employed as the current collectors of anode and cathode. As shown in Fig. 2.3a, the X-ray photoelectron spectroscopy (XPS) spectrum was obtained

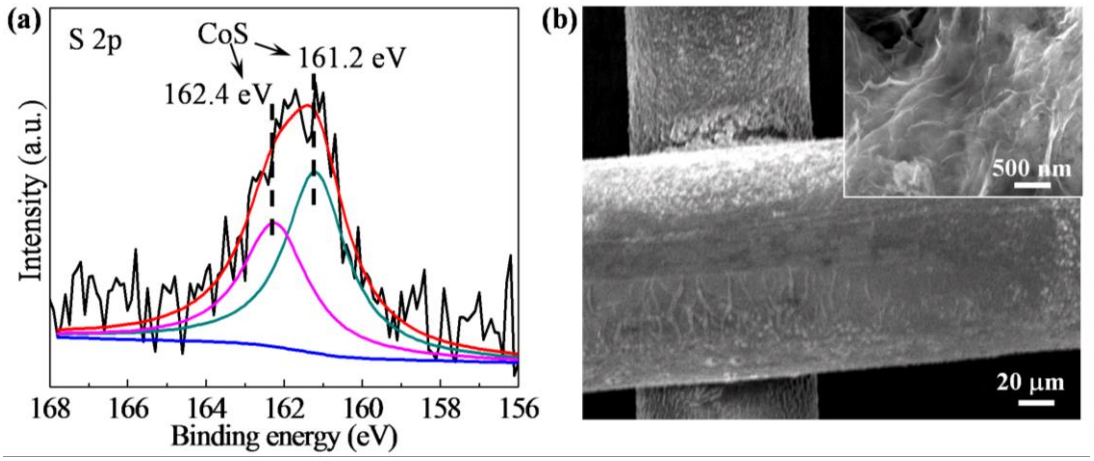

Fig. 2.3 S 2p XPS spectrum (a) and SEM images (b) of CoS deposited on a brass mesh.

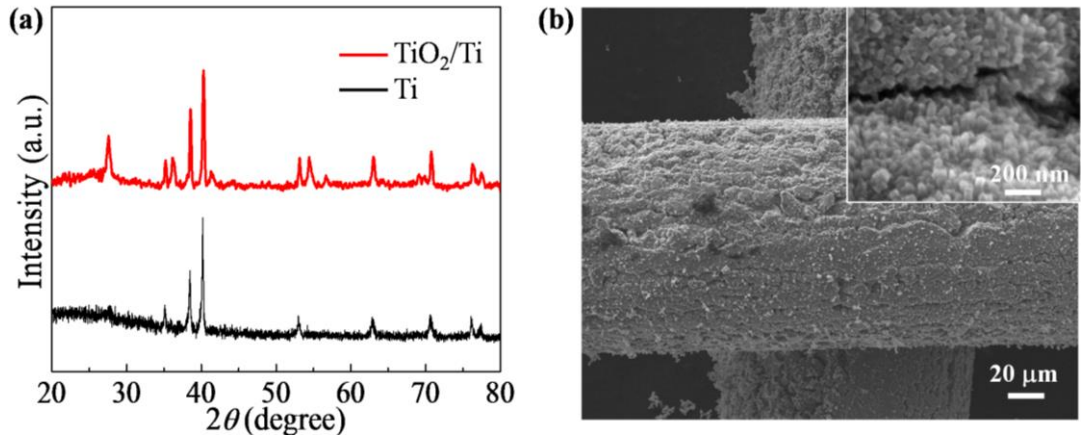

Fig. 2.4 XRD patterns (a) and SEM images (b) and of TiO_2 grown on a Ti mesh.

for investigating the chemical states of S in the CoS. Only one pair of peaks at 161.4 and 162.2 eV are assigned to the S 2p1/3 and S 2p2/3 of CoS. From the scanning electron microscopy (SEM) images in Fig. 2.3b, the prepared CoS nanosheets are

closely deposited on a brass mesh in favor of the fast electronic transmission. The crystal structure and morphology of TiO_2 photoelectrode were investigated by scanning electron microscopy (SEM) and X-ray diffraction (XRD) analysis as shown in Fig. 2.4. The prepared TiO_2 photoelectrode is rutile-phase TiO_2 nanorods grown on a Ti mesh.

2.3.2 Electrochemical performance without illumination

Before the photoassisted chargeable SPIB fabricated, we first investigated the performance of simple SPIBs. In the simple SPIB, the CoS/brass mesh and Super P/Ti mesh were employed as the current collectors of anode and cathode, respectively. The galvanostatic charge/discharge measurement has been conducted at a current density of 0.5 mA cm^{-2}. The gradient of electrolyte color suggests the depth of charge/discharge and reversibility for the SPIB as displayed in Fig. 2.5a. The galvanostatic charge/discharge curve of SPIB is shown in Fig. 2.5b with the 0.03 M Na_2S_4 and 0.15 M NaI at a current density of 0.5 mA cm^{-2}. An average charging voltage of 1.09 V and discharging voltage of 0.97 V are obtained for the SPIB, on basis of the following electrochemical equation (1) and (2):

$$\text{Anolyte: } Na_2S_4 + 6Na^+ + 6e^- \leftrightarrow 4Na_2S \quad (1)$$

$$\text{Catholyte: } 3NaI \leftrightarrow NaI_3 + 2Na^+ + 2e^- \quad (2)$$

The SPIB delivers the high charge and discharge specific capacities of 125 and 110 mAh g^{-1}, which could be calculated based on the active mass of NaI in the catholyte.

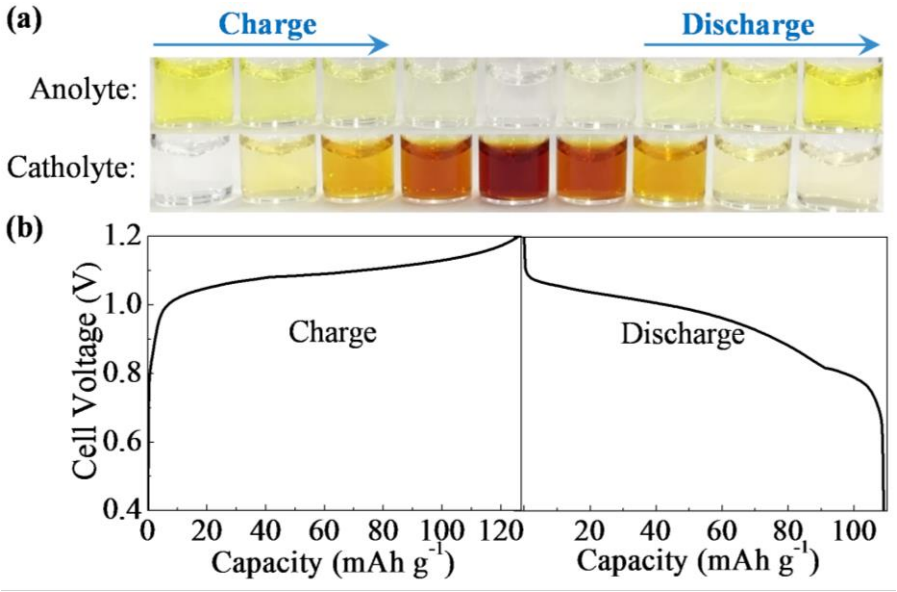

Fig. 2.5 (a) A visual color gradient of anolyte and catholyte in the SPIB during charge and discharge process. (b) Charge and discharge curves of SPIB at a current density of 0.5 mA cm^{-2}.

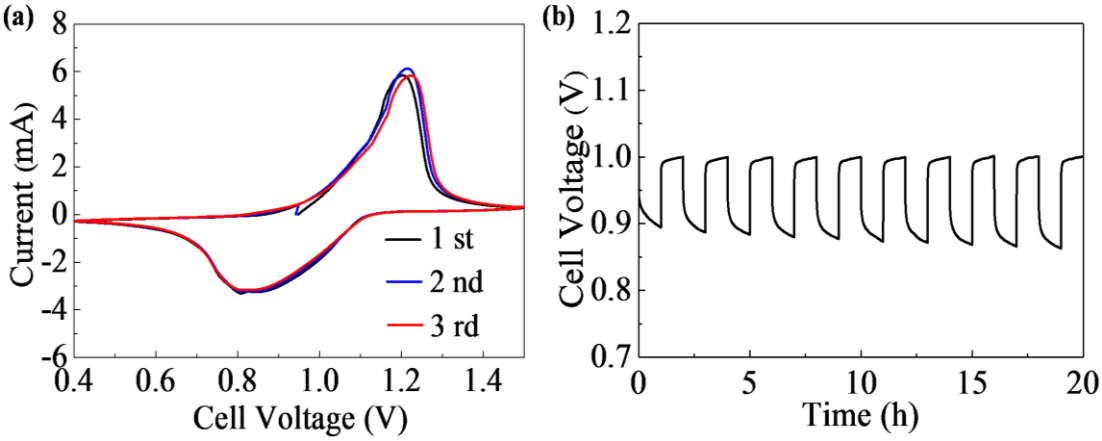

Fig. 2.6 (a) CV curves of SPIB at a sweep rate of 0.1 mV s^{-1}. (b) Charge and discharge curves of SPIB with the charging time for 1 h at a current density of 0.1 mA cm^{-2}.

The electrochemical performance of SPIB was investigated by cyclic voltammograms (CV) shown in Fig. 2.6a. CV of SPIB with the 0.1 M Na_2S_4 and 0.5 M NaI between 0.4-1.5 V at a sweep rate of 0.1 mV s^{-1} shows one pair of cathodic peak at 0.84 V and anodic peak at 1.2 V corresponding to the reduction and oxidation reaction of S_4^{2-}/S^{2-} and I_3^-/I^- redox couple, demonstrating that the anolyte and catholyte can keep the staged transformation during the charging and discharging process. It should be noted that all the CV curves overlap relatively well, and no significant peak position or intensity changes were observed for the initial three cycles, indicating the high electrochemical stability of the cell. For further investigating the stability of SPIB at a long time, the voltage-time cycling performance has been obtained Fig. 2.6b. After the 10 cycles continuing charge and discharge for nearly 20 h at a current density of 0.1 mA cm^{-2}, the battery delivered about 97% discharging voltage retention and 100% charging voltage retention, which is superior to the reported sodium polysulfide/bromine battery.[86]

2.3.3 Feasibility analysis of photoassisted charge

Having carried out performance evaluation for SPIB, a photoassisted chargeable SPIB was fabricated by incorporating the rutile-phase TiO_2 nanorods grown on a Ti mesh as a photoelectrode. Fig. 2.7a presents a light response curve of our battery. The photoassisted charging voltage increased rapidly from 0.08 to 0.86 V when the light was switched off, and it reduced to 0.08 V when the light was switched on, the instant light response not only supports our proposed working mechanism for the photoassisted charging process, but also indicates the fast reaction of photoexcited holes and electrons by using the aqueous anolyte and catholyte. In order to investigate the compositional variation of Na_2S_4 and NaI electrolytes of battery during

photoassisted charging process, the anolyte and catholyte after the photoassisted charging for 1h were analyzed by the UV-visible absorption spectroscopy. For the catholyte, there are two peaks at 288 and 350 nm assigned to I_3^- ions, demonstrating that the I^- ions are oxidized to I_3^- ions by photoexcited holes from the photoelectode.[87] On the other hand, in the anolyte three peaks at 230, 300 and 380 nm are assigned to S^{2-}, S_2^{2-} and S_4^{2-}, suggesting that the S_4^{2-} ions are reduced to the S^{2-} and S_2^{2-}.[88] These results further verify the photoassisted charging process.

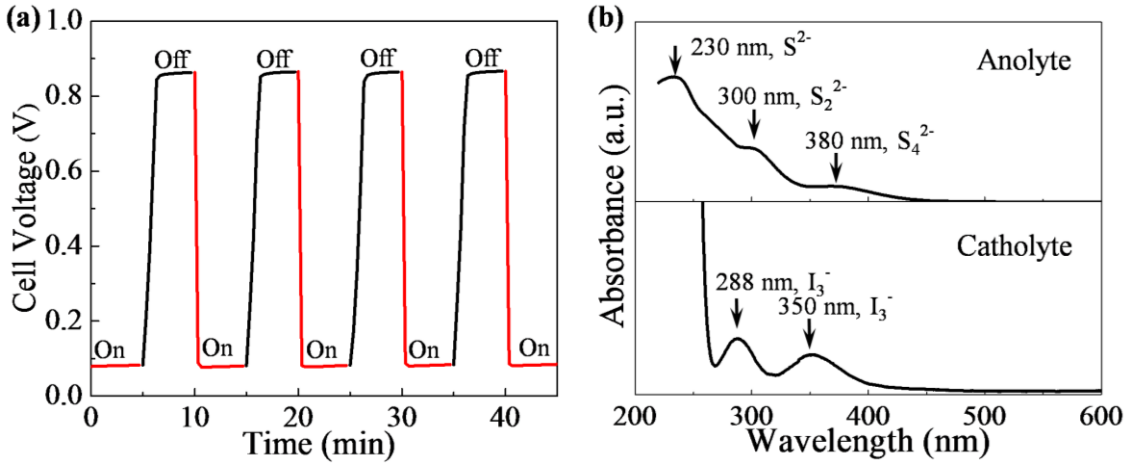

Fig. 2.7 (a) Light-response of the charge voltage of a photoassisted rechargeable SPIB when illumination was switched from "on" to "off". (b) UV-visible absorption spectra of anolyte and catholyte after the photoassisted charging for 1 h.

Fig. 2.8 exhibit the comparisons of charging and discharging profiles between the photoassisted chargeable SPIB and conventional SPIB with the 0.03 M Na_2S_4 and 0.15 M NaI. When the photoassisted chargeable SPIB was charged under the illumination at a current density of 0.01 mA cm^{-2} for 1 h, the charging voltage was dramatically reduced to 0.08 V, obviously lower than that of conventional SPIB (0.86 V). The

ultralow voltage value matches well with the theoretical prediction (0.07 V), indicating that the aqueous electrolyte system has small internal resistance in favor of the photoelectric conversion of the TiO_2 photoelectrode. The photoassisted chargeable SPIB can save ～90% input electric energy with the aid of solar energy, which is thermodynamically impossible for any conventional redox batteries. Energy saving efficiency is calculated based on the difference between the charge and photoassisted charge voltages at the half-charge capacity point ((0.86 V - 0.08 V)/0.86 V × 100% = 90%). Moreover, the smooth voltage plateau also embodies the durability of the photo-electric conversion.

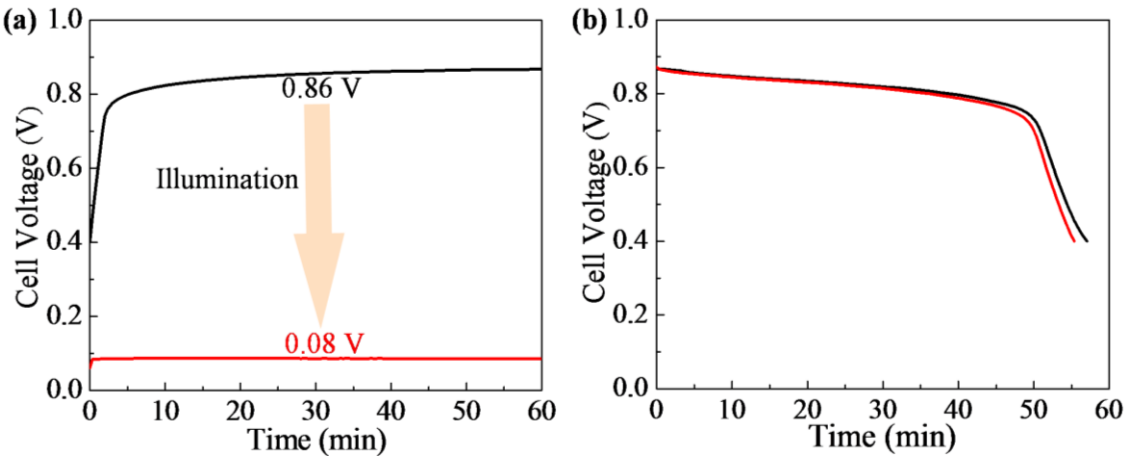

Fig. 2.8 Charge curves (a) and (b) discharge curves of photoassisted rechargeable SPIB (red line) and the SPIB (black line) at a current density of 0.01 mA cm^{-2}.

2.3.4 Photoassisted electrochemical performance

The charge/discharge curves of photoassted rechargeable SPIB at different current densities are shown in Fig. 2.9. Although it is noted that the polarization trends of charging voltage increased slightly with the variation of current densities, the voltage

plateau is still recorded as 0.13 V even at a current density of 0.03 mA cm^{-2} (Fig. 2.9a). while the corresponding discharge time is closed to 160 min.

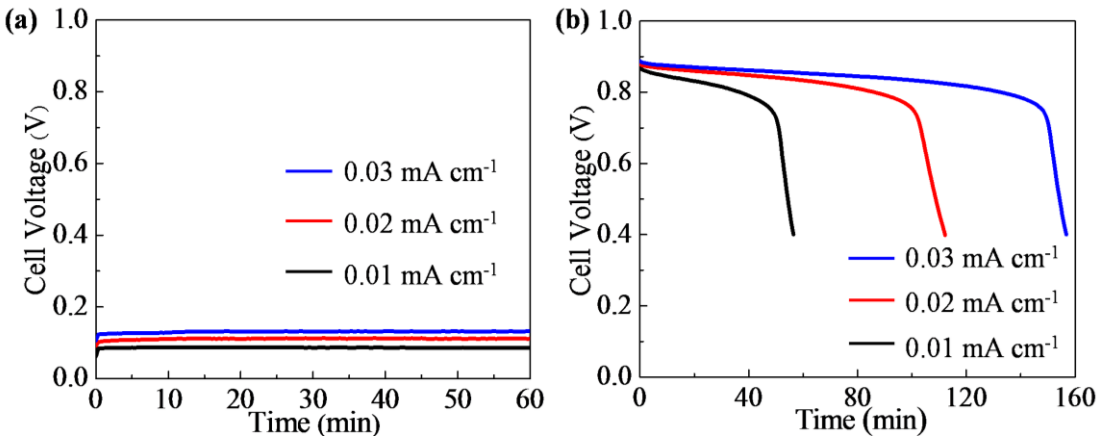

Fig. 2.9 (a) Charge curves of photoassisted rechargeable SPIB at different current densities. (b) Corresponding discharge curves at a uniformly current density of 0.01 mA cm^{-2}.

The cycling stability of photoassisted chargeable SPIB is also evaluated by the galvanostatic charge and discharge measurement. The total 20 cycle voltage profiles as well as the enlarged 1st and 20 th cycle voltage profiles are as shown in the Fig. 2.10. The red and black curves in the figures represent, respectively, the photoassisted charge and discharge voltage profiles. The initial photoassisted charging voltage is 0.08 V, contributing to an input electric energy saving of ~90%. After 20 cycles, the battery still delivered 0.1 V charging voltage, contributing to saving ~88% input electric energy, suggesting the good stability of the system.

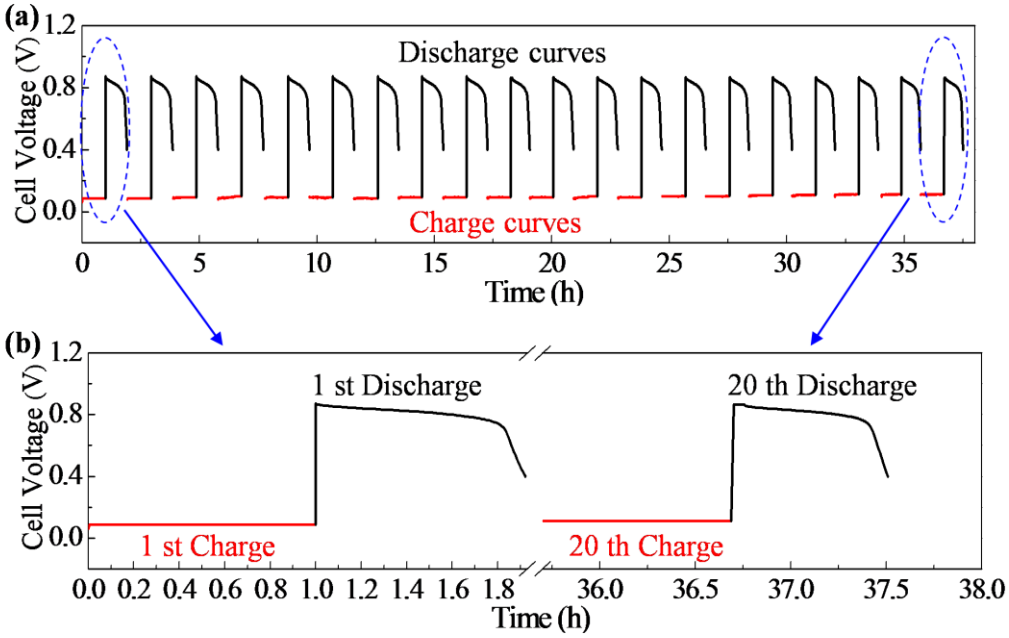

Fig. 2.10 (a,b) Charge and discharge curves at a current density of 0.01 mA cm^{-2} of photoassisted rechargeable SPIB under the illumination for 1 h.

The electrochemical properties of photoassisted rechargeable SPIB have been further investigated at a high current density for a long time. In Fig. 2.11, the charge and discharge curves of the photoassisted chargeable SPIB have been obtained with the 0.01 M Na_2S_4 and 0.005 M NaI at a current density of 0.05 mA cm^{-2} for 4 h. The battery can still remain a long charge voltage plateau at 0.18 V and deliver the discharging capacity of 110 mAh g^{-1}. Through combining a flow-through-mode system, the performance of photoassisted chargeable SPIB can be further improved

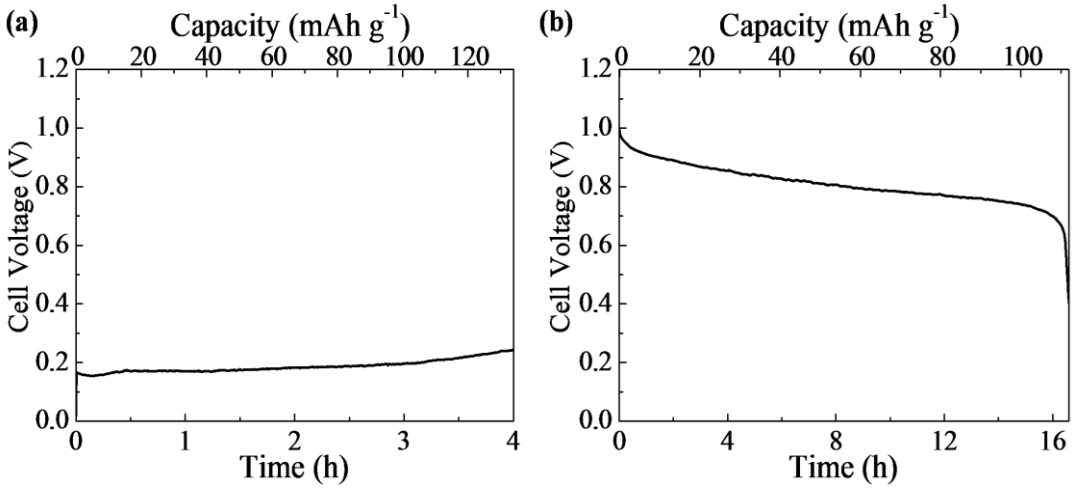

Fig. 2.11 (a) Charge curves of photoassisted rechargeable SPIB at a current density of 0.05 mA cm^{-2}. (d) Corresponding discharge curves at a current density of 0.01 mA cm^{-2}.

2.4 Conclusions

In summary, by utilizing a photoassisted charging strategy, the simultaneous conversion and storage of solar energy in aqueous the battery firstly have been demonstrated in a novel photoassisted rechargeable SPIB. This battery employs the aqueous anolyte and catholyte as the active materials, and a TiO_2 photoelectrode is integrated into the catholyte side for capturing solar energy. Due to the compensation of photovoltage, this photoassisted rechargeable can be charged at an ultralow charging voltage of 0.08 V, which realize the ~ 190% energy conversion efficiency, equal to saving ~ 90% input electric energy. This full aqueous photoassisted rechargeable battery provides the potential route for promoting the practical application of high-safety and low-cost rechargeable batteries by the photo-driven.

Chapter 3. A photoassisted rechargeable organic battery

3.1 Introduction

The conversion/storage of solar energy in high-voltage organic batteries are expected for the large-scale applications. The P2 phase layer metal oxides have attracted wide attention due to its safe voltage and excellent electrochemical performance.[89, 90] While NaI_3/NaI redox couples has a high voltage, and ions are more easy to be motivated by the photoecatalysis.[91] Therefore, employ the P2 phase metal oxide and NaI_3/NaI redox couple as anode and cathode will assemble a low-cost and high voltage organic sodium-ion battery (SIB). For the photoelectrode, the photocatalysts on the photoelectrode play the important role in the photoassisted chargeable batteries. In the past few years, there have been significant efforts to develop novel photocatalysts for the solar energy conversion and storage. Although many photocatalysts that function efficiently under ultraviolet (UV) irradiation have been developed such as TiO_2, only a few visible light driven photocatalysts have been reported for solar energy conversion and storage devices. To efficiently utilize solar energy, however, compounds with absorption bands at the longer wavelengths are required. There have been some reports that (oxy)nitrides of early transition metals with d^0-electronic configurations are potential candidates for visible light absorption such as the Tantalum nitride (Ta_3N_5). Ta_3N_5 with a band gap of 2.1 eV (absorption edge at 600 nm) has conduction and valence band edges at ca.-0.4 and +1.7 V *vs* NHE, respectively.[92-94] In this work, we propose a photoassisted chargeable sodium-iodine battery (SIB), which employs P2-$Na_{0.66}Ni_{0.17}Co_{0.17}Ti_{0.66}O_2$ and NaI/NaI_3 as the active materials of anode and cathode respectively, and a Ta_3N_5 photoelectrode integrated into the catholyte for realizing the visible light-driven. Under the visible light radiation, the

charging voltage of photoassisted chargeable SIB with Ta_3N_5 photoelectrode has been reduced to 1.65 V compared with the photoassisted chargeable SIB integrated by the TiO_2 photoelectrode. This full organic photoassisted chargeable SIB driven by the visible light broadens the actual application of the devices under the solar radiation spectrum.

3.2 Experiment and characterization

3.2.1 Preparation of anode material, separator and photoelectrode

P2-$Na_{0.66}Ni_{0.17}Co_{0.17}Ti_{0.66}O_2$ as anode material was prepared on basis of a modified solid-state calcination.[95] The precursors of Na_2CO_3, NiO, CoO and TiO_2 (Wako company) were mixed with a stoichiometric ratio, and the Na_2CO_3 of a 5 wt.% excess was added for compensating the loss of sodium source. The precursors were ball-milled with alcohol additions for 12 h at 100 rpm. After drying at 80 °C for 12 h, the obtained powder was pressed into pellets. The pellets were firstly heated at 900 °C for 15 h under an Ar atmosphere. Finally, the heated pellets were quenched to room temperature and the sealed pellets were stored in an argon-filled glove box until the next using.

PNP separator was prepared by a modified two-step method: the manual lamination and the sequent ion exchange.[96] Firstly, a certain volume of Nafion 117 solution (Sigma-Aldrich, ~5 wt% in a mixture of water and aliphatic alcohols,) was uniformly coated on the surface of a Celgard 2400 membrane (microporous polypropylene membrane). When the Nafion layer became sticky after natural drying in the air, another Celgard 2400 membrane was evenly pressed on the surface of Nafion layer. The sandwich-type membrane was dried at 60 °C in vacuum to completely evaporate the solvents and then cut into disks. These disks were subsequently immersed in 1 M NaTFSI ($NaN(CF_3SO_2)_2$, Aldrich) solution in DME (Wako, dried by 4 Å molecular

sieve) for 24 h for sufficient H^+–Na^+ ion-exchange, washed with DME, and then naturally dried in glove box.

Ta_3N_5 photoelectrode was prepared by a modified thermal oxidation and subsequent nitridation method.[94] Firstly, a Ta mesh was cut into 1×1 cm^2 pieces and cleaned in ethanol and acetone. Then, Ta meshes were oxidized at a temperature of 550 °C in air for 30 min, and then were nitrided at 850 °C for 8 h under a flow of ammonia gas (500 mL min^{-1}) to form Ta_3N_5 nanorods on the surface of Ta meshes.

TiO_2 photoelectrode was prepared for comparison with Ta_3N_5 photoelectrode, and the method is similar with the above work. Through a hydrothermal method at 170 °C for 10 h in a $TiCl_4$ (99.0%, Aldrich) and HCl (37%, Wako) mixed solution, the initial nanorods TiO_2 was deposited on pretreated Ti mesh, and the subsequent calcination at 450 °C for 2 h was used to improve its crystallinity.

3.2.2 Assembly of photoassisted rechargeable organic battery

Photoassisted rechargeable SIB consists of a P2-$Na_{0.66}Ni_{0.17}Co_{0.17}Ti_{0.66}O_2$ anode with organic electrolyte, a PNP separator, a NaI_3 cathode with organic electrolyte, and a Ta_3N_5 photoelectrode (Fig. 3.1). The P2-$Na_{0.66}Ni_{0.17}Co_{0.17}Ti_{0.66}O_2$ anode was prepared by mixing the P2-$Na_{0.66}Ni_{0.17}Co_{0.17}Ti_{0.66}O_2$ with teflonized acetylene black and polytetrafluoroethylene (PTFE) in a weight ratio of 75:20:5. The resulting slurry was then cast on a Ti mesh, then dried under vacuum at about 100 °C for 24 h before cells assembly. A RGO (Product No: GNIP0005, ACS MATERIAL company) electrode as current collector of cathode was prepared by coating a slurry of RGO and PTFE in a weight ratio of 80:20, then dried under vacuum at about 100 °C for 24 h before cells assembly. The prepared PNP separator was sealed on the middle of two glass cylinders which were respectively fixed by the anode and cathode sides. A 1 M

$NaClO_4$ organic electrolyte with tetraglyme (G4) as solvent was employed as the anolyte, white NaI was solved in 1 M $NaClO_4$ organic electrolyte with G4 solvent as the catholyte. For strictly avoiding the external contamination, the entire battery was assembled in an Ar-filled glove box (<1 p.p.m. of H_2O and O_2).

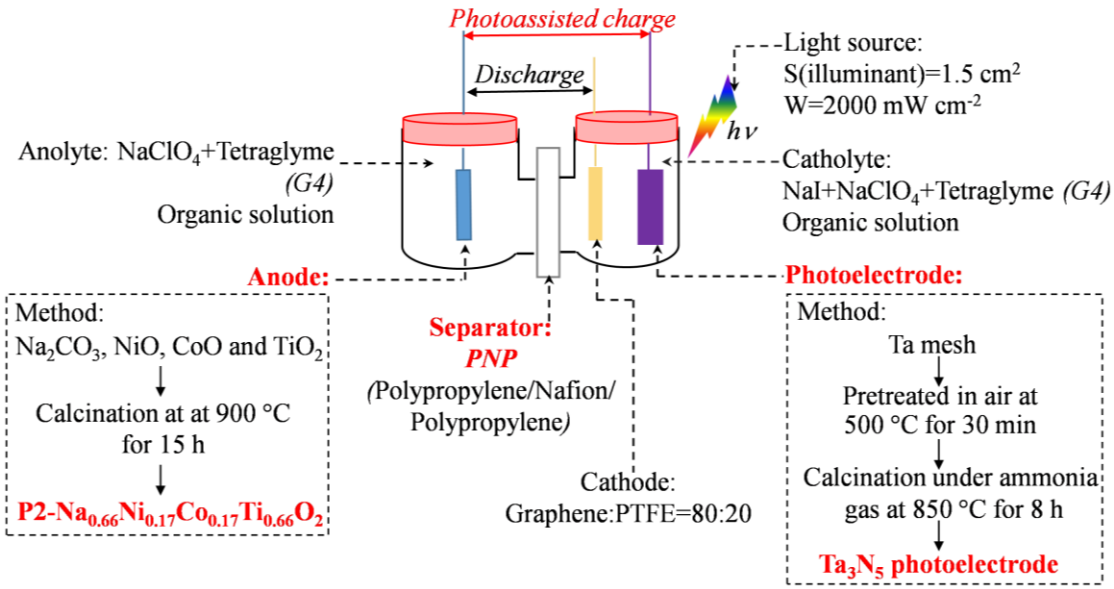

Fig. 3.1 Fabrication of a photoassisted rechargeable organic SIB.

3.2.3 Electrochemical and photoelectrochemical measurements

The light source used for the illumination is a XEF-501S Xe-lamp (San-ei Electric Co., Japan). The charging/discharging tests for the total batteries were performed at different current densities by using a Hokuto electrochemical machine. For a photoassisted rechargeable organic SIB, the photoelectrode and anode were directly connected on the electrochemical machine during the charge under illumination, and the cathode and anode were connected for the discharge without illumination. For the

rechargeable organic SIB without illumination, the cathode and anode were connected by electrochemical machine during the charge and discharge.

3.2.4 Characterizations

The morphology was observed by using a scanning electron microscope of Hitachi S4800. The crystal structures were characterized by the employment of a Bruker D8 advanced diffractometer with Cu Kα (λ = 1.5406 Å) radiation. The UV-visible absorption spectrum measurements were carried out on a Shimadzu UV3101PC. The Fourier Transform Infrared Spectroscopy (FT-IR) were performed by employing a JASCO instrument of FT/IR-6200.

3.3 Results and discussion

3.3.1 Design of a photoassisted rechargeable organic battery

A photoassisted rechargeable organic SIB is designed for achieving the conversion and storage of solar energy in rechargeable organic battery. Fig. 3.2 outlines the structure of the desirable photoassisted rechargeable SIB. It consists of a P2-$Na_{0.66}Ni_{0.17}Co_{0.17}Ti_{0.66}O_2$ anode with organic electrolyte, a PNP separator, a NaI catholyte with organic electrolyte, and a Ta_3N_5 photoelectrode which is inserted into the catholyte for capturing solar energy. The charging process is conducted under illumination, and a photoassisted voltage is applied on the P2-$Na_{0.66}Ni_{0.17}Co_{0.17}Ti_{0.66}O_2$ anode and Ta_3N_5 photoelectrode. Detailedly, upon charging under illumination, the photoexcited holes (h^+) in the valence band (VB) of the Ta_3N_5 photoelectrode can oxidize NaI into NaI_3 in the catholyte. At the same time,

the photoexcited electrons (e^-) in the conduction band (CB) of photoelectrode transfer into anode for reducing $Na_{0.66}Ni_{0.17}Co_{0.17}Ti_{0.66}O_2$ to $Na_{0.66+x}Ni_{0.17}Co_{0.17}Ti_{0.66}O_2$ by external circuit. Consequently, the photovoltage generated on the Ta_3N_5 photoelectrode compensates the battery's charging potential. During the discharging process, the anode and cathode are connected to the output clients, and the reduction from NaI_3 to NaI and the oxidation from $Na_{0.66+x}Ni_{0.17}Co_{0.17}Ti_{0.66}O_2$ to $Na_{0.66}Ni_{0.17}Co_{0.17}Ti_{0.66}O_2$ are operated respectively in the cathode and anode, which are similar with the conventional SIB without the illumination. The entire photoassisted charge and discharge process are shown in the following equations:

Photoassisted charge: $h\nu \rightarrow Ta_3N_5 \rightarrow h^+ + e^-$ (photoelectrode)

$$2h^+ + 3NaI \rightarrow NaI_3 + 2Na^+ \quad \text{(cathode)}$$

$$x Na^+ + Na_{0.66}Ni_{0.17}Co_{0.17}Ti_{0.66}O_2 + x e^- \rightarrow Na_{0.66+x}Ni_{0.17}Co_{0.17}Ti_{0.66}O_2 \text{ (anode)}$$

Discharge: $NaI_3 + 2Na^+ + 2e^- \rightarrow 3NaI$ (cathode)

$$Na_{0.66+x}Ni_{0.17}Co_{0.17}Ti_{0.66}O_2 \rightarrow Na_{0.66}Ni_{0.17}Co_{0.17}Ti_{0.66}O_2 + x Na^+ + x e^- \text{ (anode)}$$

Due to the compensation of solar energy, the photoassisted charge potential equals the energy difference between the redox potential of the P2-$Na_{0.66}Ni_{0.17}Co_{0.17}Ti_{0.66}O_2$ and the quasi-Fermi level of the electrons in the Ta_3N_5 photoelectrode (which is near to the conduction band (CB) of the Ta_3N_5) as presented in Fig. 3.2b. Since the CB potential of Ta_3N_5 (~2.31 V *vs* Na/Na^+) is lower than the NaI/NaI_3 standard potential of ~2.72 V *vs* Na/Na^+,[93] the photoassisted charge voltage is expected to be lower than that of conventional $Na_{0.66}Ni_{0.17}Co_{0.17}Ti_{0.66}O_2$/NaI batteries.

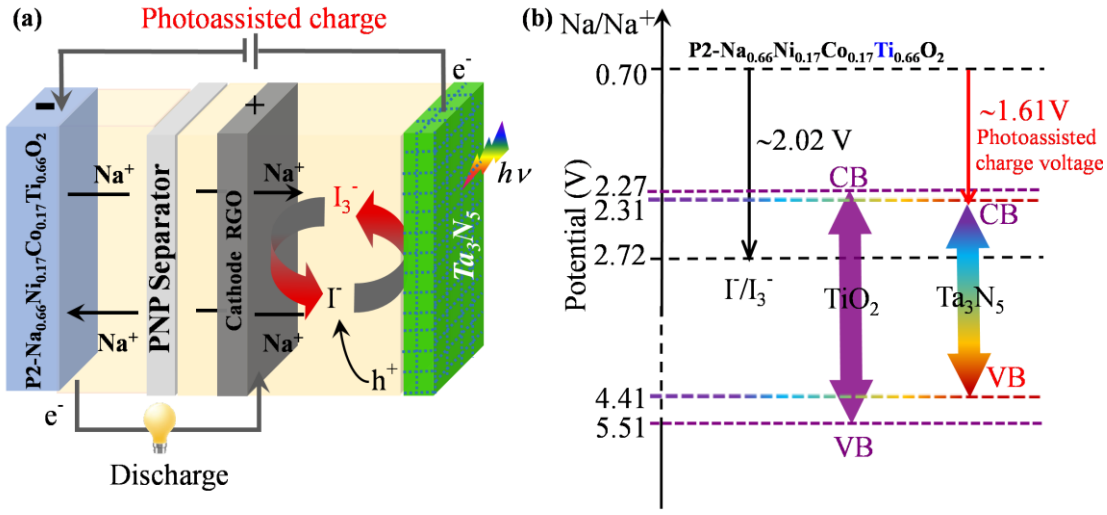

Fig. 3.2 (a) Schematic of a photoassisted rechargeable organic SIB. (b) Potential diagram for the photoassisted charging process. The photoassited charge voltage is determined by the energy difference between anode voltage of SIB and quasi-Fermi level of electrons in the Ta_3N_5 photoelectrode (near to its conduction band (CB)).

In this designed photoassisted rechargeable organic SIB, P2-$Na_{0.66}Ni_{0.17}Co_{0.17}Ti_{0.66}O_2$ anode material is prepared by a modified solid-state calcination based on the Na_2CO_3, NiO, CoO and TiO_2 as precursors. The crystal structure and morphology of prepared $Na_{0.66}Ni_{0.17}Co_{0.17}Ti_{0.66}O_2$ are characterized by the X-ray diffraction (XRD) and scanning electron microscope (SEM). As shown in the XRD pattern of sample in Fig. 3.3a, all the diffraction lines can be indexed to a hexagonal lattice with space group P63/mmc which is consistent with the reported literature,[95] indicating the prepared sample is attributed to the P2-phase layer material. Meanwhile, the high diffraction intensity of peaks suggests that the prepared sample has a good crystallinity. Fig. 3.3b displays the SEM image of the prepared sample. It can be seen that the prepared $Na_{0.66}Ni_{0.17}Co_{0.17}Ti_{0.66}O_2$ are some particles, and the sizes range from 2 to 5 μm.

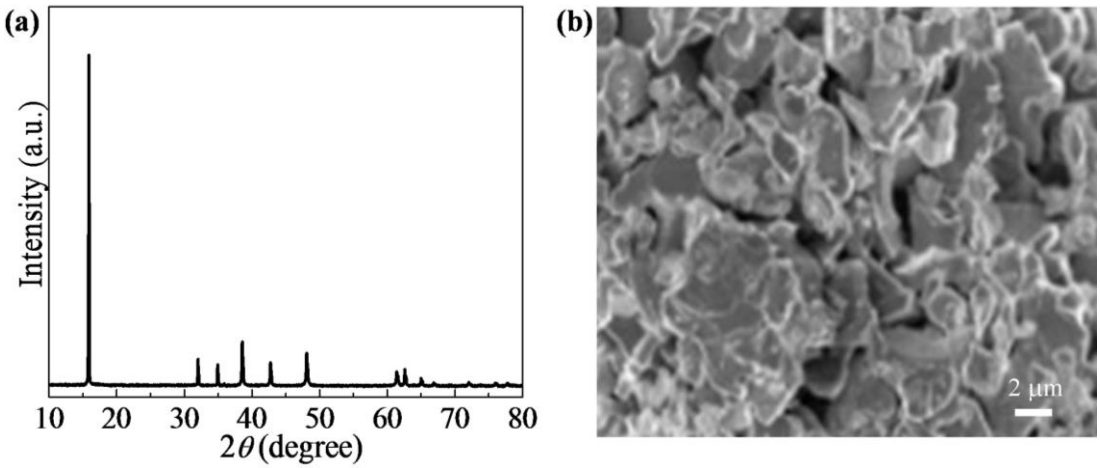

Fig. 3.3 XRD pattern (a) and SEM image (b) of P2-$Na_{0.66}Ni_{0.17}Co_{0.17}Ti_{0.66}O_2$.

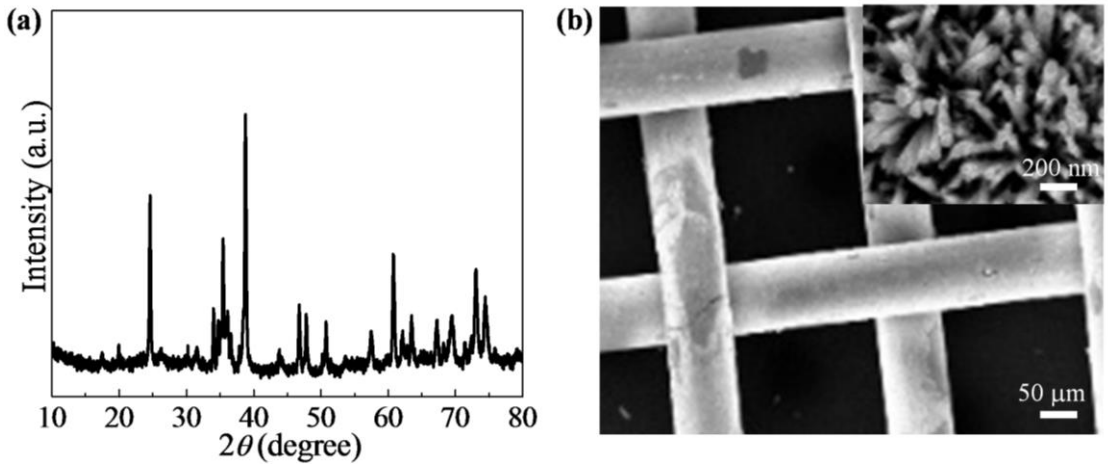

Fig. 3.4 XRD pattern (a) and SEM images (b) of Ta_3N_4 photoelectrode (b high-magnification SEM image is shown as the inset).

The photoelectrode of photoassisted rechargeable organic SIB is prepared by a modified thermal oxidation and subsequent nitridation method on Ta mesh.[94]

Through employing the XRD and SEM characterizations, the crystal structure and morphology of prepared photoelectrode have been demonstrated as shown in Fig 3.4. The result of XRD pattern displays that all the diffraction peaks are assigned to the Ta_3N_5 and Ta mesh, which is consistent with reported literature,[94] suggesting the Ta_3N_5 has been successfully prepared. The SEM images of Ta_3N_5 photoelectrode are presented in Fig. 3.4b. It can be observed that the surface of Ta mesh is compactly coated by Ta_3N_4, and the morphologies of Ta_3N_4 are nanorods with the diameter of ~ 20 nm. The uniform Ta_3N_4 nanorods grown on the surface of Ta mesh are more benefit to the fast transfer of the electrons.

For overcoming the shuttle-effect of catholyte and improving the electrochemical performance of rechargeable organic SIB, A Na^+-PNP separator enabling the Na^+ migration has been firstly prepared by a modified sandwich-type superposition method.[96] The Na^+-PNP separator includes the three layers of polypropylene (Celgard), Nafion and polypropylene (Celgard). Especially, the middle Nafion layer cation not only enable to permselective the Na^+ ions, but also can block the shuttle of molecules and organic electrolytes. According to the reported findings,[96] the Li-ion batteries with H-Nafion as separator have the large voltage polarization because of the seriously increased viscosity in the electrolyte solution with the presence of H^+ released from the H-Nafion during the electrochemical process. Therefore, the prepared H-PNP separators are need to be immersed in 1 M NaTFSI/DME solution for the sufficient ion-exchange between Na^+ and H^+ ions. The structures of simple Celgard and Na^+-PNP separator have been characterized by Fourier transform infrared spectroscopy (FT-IR) in Fig. 3.5a. In comparison with the FT-IR spectrum of Celgard, the strong absorptions between 1300 and 1100 cm^{-1} for Na^+-PNP separator clearly demonstrate the presence of Nafion layer.[97] While, the absorption peak appears at 1638 cm^{-1} strongly proving that the H^+ ions have been ion-exchanged with Na^+.[98]

Then, the block effect of Na^+-PNP separator has been proved by a long-time permeation experiment as shown in Fig. 3.5b. The left side to cylinder is fixed with NaI_3 + $NaClO_4$ + G4 organic solution, while the right side is only $NaClO_4$ + G4 organic solution. After different standing time, the images of this device have been remembered, and the experiential results show the side of simple $NaClO_4$ + G4 organic solution is still colorless even after 1 week immersion, demonstrating that the prepared Na^+-PNP separator has a good blocking ability for the shuttle of I_3^- ions.

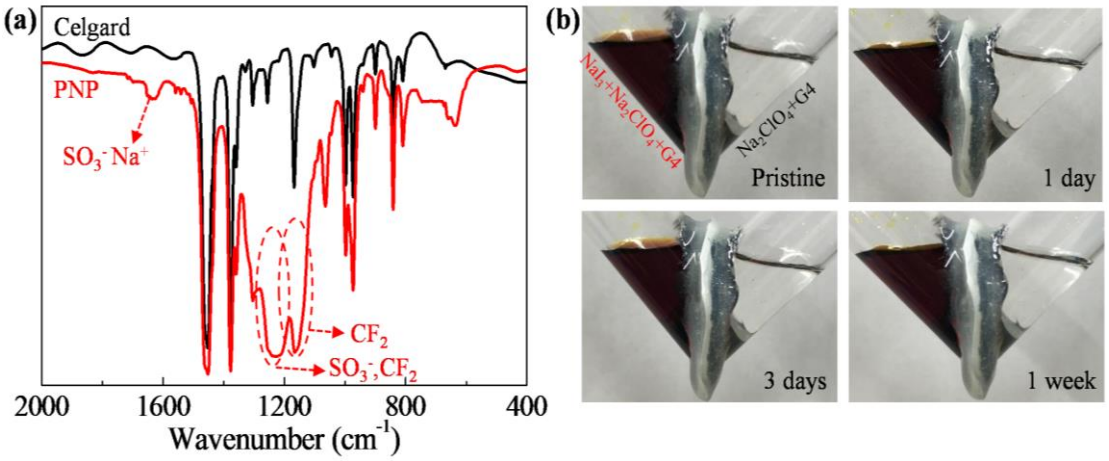

Fig. 3.5 (a) IR spectra of Celgard and PNP separator. (b) Permeability of PNP separator.

3.3.2 Electrochemical performance without illumination

The electrochemical performance of the assembled rechargeable organic SIB without illumination has been evaluated by the galvanostatic charge/discharge measurements. Fig. 3.6a displays the typical discharge/charge curves of the sample at a current density of 0.2 mA cm^{-2} with the voltage range of 1.0–3.8 V. It can be observed that this organic full-cell presents two redox voltage-platforms at ~ 2.7 V and 2.0 V (average discharging voltage-platform) which should be attributed to the

transformations of I_2/I_3^- and I_3^-/I^- two couples.[99] Meanwhile, the cell delivers a reversible capacity of 193 mAh g^{-1} in the discharge of first cycle and still maintains a good cycling performance after 5 cycles. The long-term cycling performance is further investigated for 200 cycles at a current density of 0.2 mA cm^{-2}. The result in Fig. 3.6b displays that the discharging capacity changes from 193 mAh g^{-1} to 183 mAh g^{-1}. An excellent capacity retention of 94% is obtained after 200 cycles, which corresponds to a capacity fading of only 0.025% per cycle.

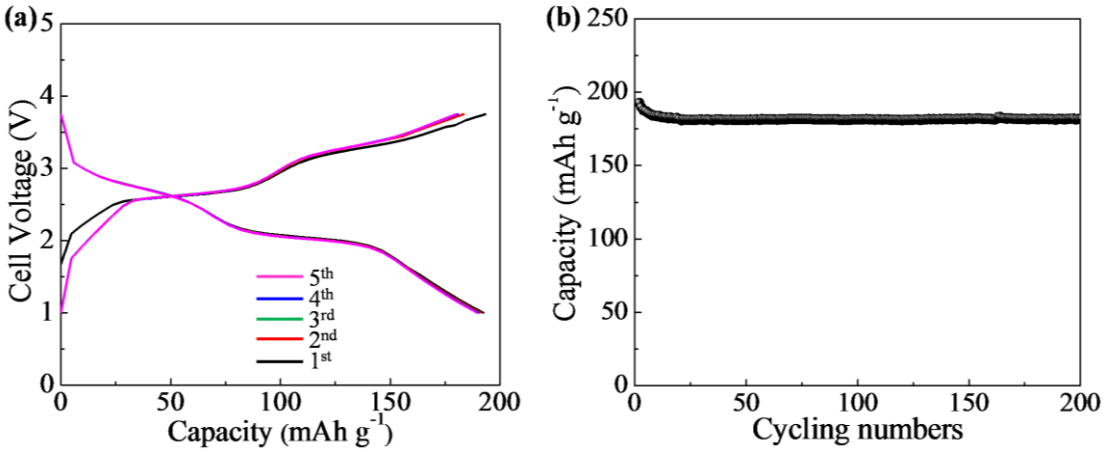

Fig. 3.6 (a) Charge and discharge curves of SIB without illumination from first cycle to 5^{th} cycle at a current density of 0.2 mA cm^{-2}. (b) Cycling performance after 200 cycles at a current density of 0.2 mA cm^{-2}.

The rate with cycling performance is presented in Fig. 3.7. The reversible discharge capacities of 199, 166, 124, 79 and 57 mAh g^{-1} are obtained at the current densities of 0.2, 0.4, 0.6, 0.8, and 1 mA cm^{-1}, respectively. When the current density returns to 20 mA cm^{-1}, the discharge capacity comes back to 194 mAh g^{-1}, which suggesting the good cycling stability of the assembled full cell.

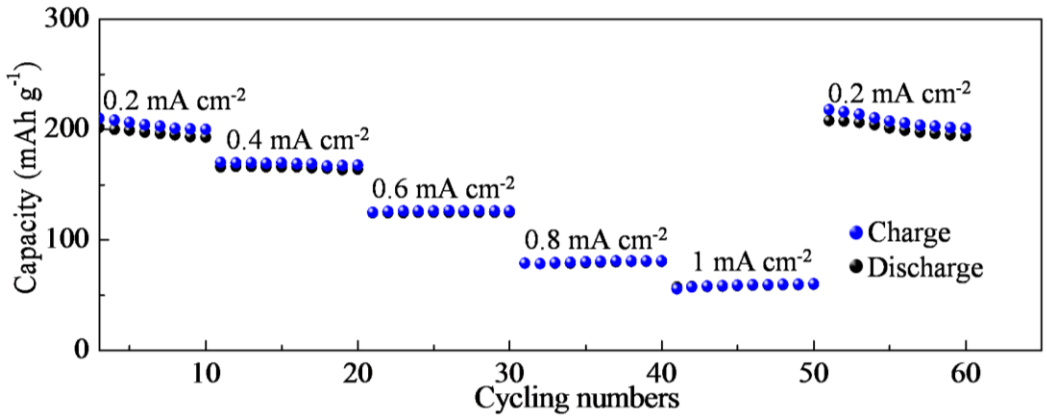

Fig. 3.7 Rate capability and cycling performance of SIB at different current densities.

3.3.3 Feasibility analysis of photoassisted charge

To investigate the visible-light driven feasibility of assembled photoassisted SIB with Ta_3N_5 photoelectrode, a photoassisted SIB with integration of TiO_2 photoelectrode has been assembled for the comparison. From the photoassisted charge curves under visible-light radiation, it can be seen that the TiO_2 photoelectrode has no obvious light-response with the increased voltage (black line), while the battery with Ta_3N_5 photoelectrode has a low charge voltage at ~1.65 V which is closed to the theoretical value (red line). Only under the ultraviolet (UV)-light radiation, the battery with TiO_2 photoelectrode shows a low charge voltage (purple line). The photocatalytic activity of Ta_3N_5 for I^- organic solution has been verified by the ultraviolet-visible (UV-Vis) spectrum (Fig. 3.8 b). After the 1 h visible-light radiation for Ta_3N_5 photoelectrode containing I^- ions solution, the UV-Vis spectrum shows that two peaks attributed to I_3^- ions (288 and 350 nm) are identified, demonstrating the feasible photoelectrochemical oxidation reaction from I^- to I_3^- ions aided by the Ta_3N_5 photoelectrode under the visible-light radiation.

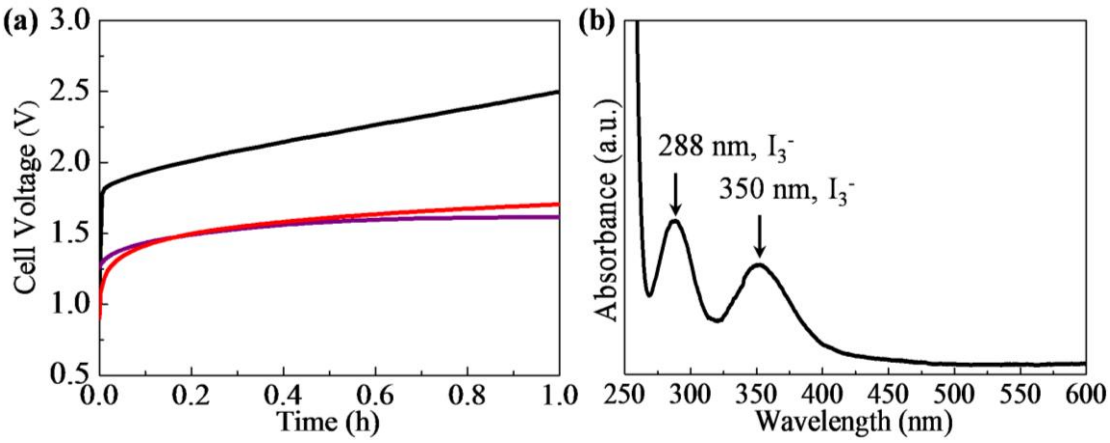

Fig. 3.8 (a) Photoassisted charge curves of different batteries with TiO_2 photoelectrode under visible light (black line), Ta_3N_5 photoelectrode under visible light (red line), and TiO_2 photoelectrode under UV light (purple line). (b) UV-Vis spectrum of I^- ions solution containing Ta_3N_5 photoelectrode after 1 h visible-light radiation.

In order to further confirm the feasibility of photoassisted organic SIB, the charge and discharge curves with illumination and no illumination have been obtained as shown in Fig. 3.9. Under the visible-light radiation, the photoassisted organic SIB can charge at a low voltage of ~1.65 V, which is obviously lower that ~2.37 V of organic SIB without the illumination. It is noticeable that this charging voltage is lower than the discharging voltage, which is thermodynamically impossible without the solar energy input. In addition, the photoassisted organic SIB is enable to discharge with a discharging time of ~1.85 h, which is similar with the conventional organic SIB. Above experimental results indicate the assembled organic SIB has a good coulombic efficiency during the visible photoassisted charge and discharge.

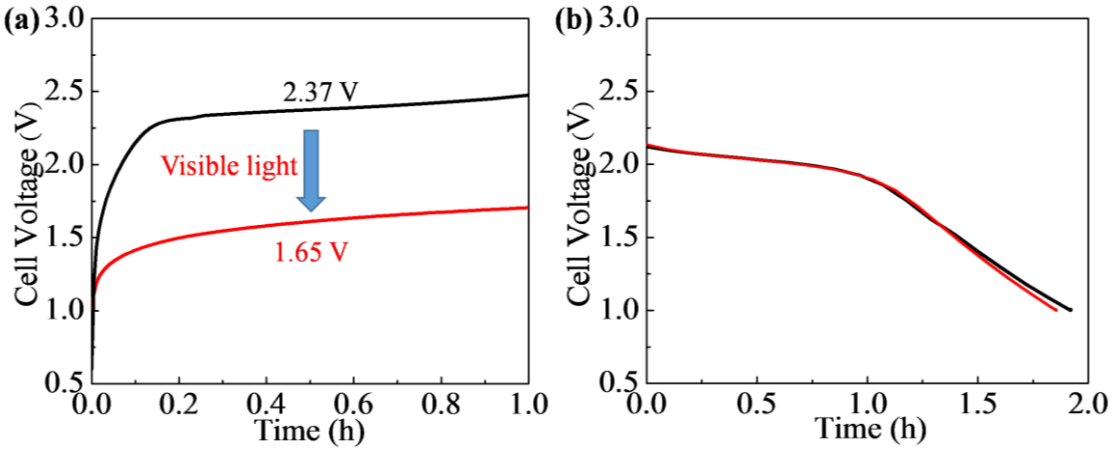

Fig. 3.9 (a) Charge curves of photoassisted rechargeable SIB (red line) and SIB (black line) at a current density of 0.02 mA cm^{-2}. (b) corresponding discharge curves at a current density of 0.01 mA cm^{-2}.

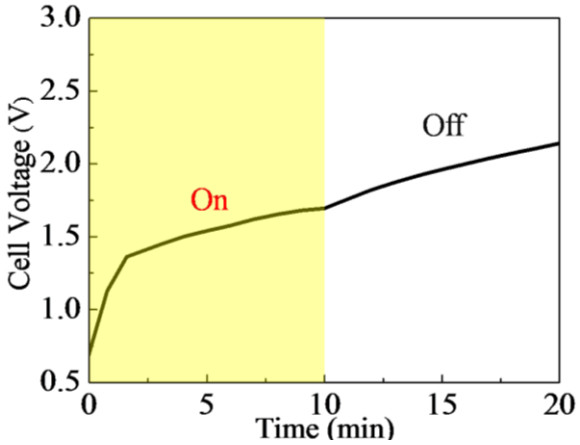

Fig. 3.10 Light-response of the charge voltage of a photoassisted rechargeable SIB when illumination was switched from "on" to "off".

A light-response of photoassisted organic SIB has been tested when the switched from "on" to "off" (Fig. 3.10). Comparing with above work in the aqueous system, the charging voltage is slowly increased when the illumination was removed. This

phenomenon could be attributed to the higher viscidity of organic system which is not in favor of the fast transfer of electrons and holes.

3.3.4 Photoassisted electrochemical performance

The charging/discharging curves of the photoassisted organic SIB at different current rates from 0.02 to 0.04 mA cm^{-2} are shown in Fig. 3.11. It is notable that the degree of polarization does not drastically increase. The photoassisted charging voltage is recorded as 1.82 V, even at the current of 0.04 mA cm^{-2}. The photoassisted organic SIB can exhibit a long discharging time at the current of 0.04 mA cm^{-2}.

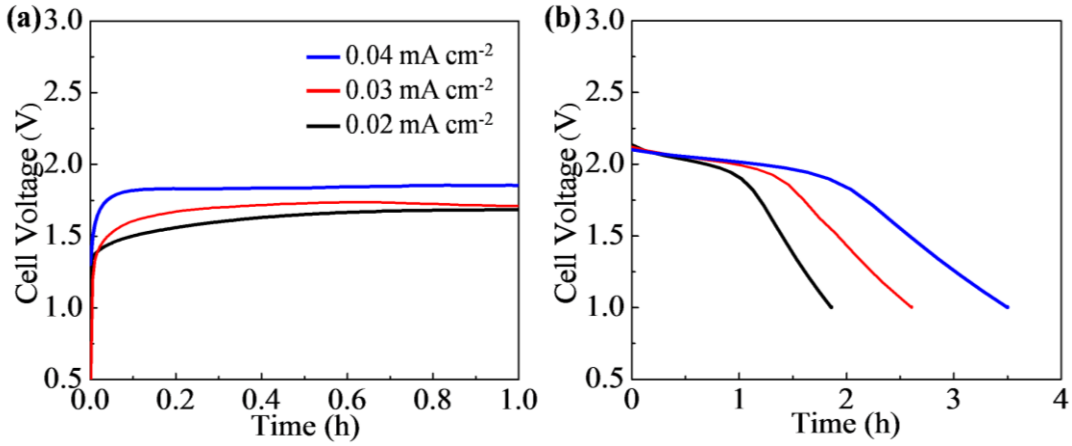

Fig. 3.11 (a) Charge curves of photoassisted rechargeable SIB at different current densities. (b) Corresponding discharge curves at a uniformly current density of 0.01 mA cm^{-2}.

The cycling stability of photoassisted rechargeable organic SIB is also evaluated by the galvanostatic charge and discharge measurement. The total 20 cycle voltage profiles as well as the enlarged 1st and 20 th cycle voltage profiles are as presented in

Fig. 3.12. The red and black curves in the figures represent, respectively, the photoassisted charge and discharge voltage profiles. The initial photoassisted charging voltage is 1.65 V, contributing to an input electric energy saving of ~14%. After 20 cycles, the battery still delivered 1.88V charging voltage with a 0.23 V increasing, suggesting the good stability of the system.

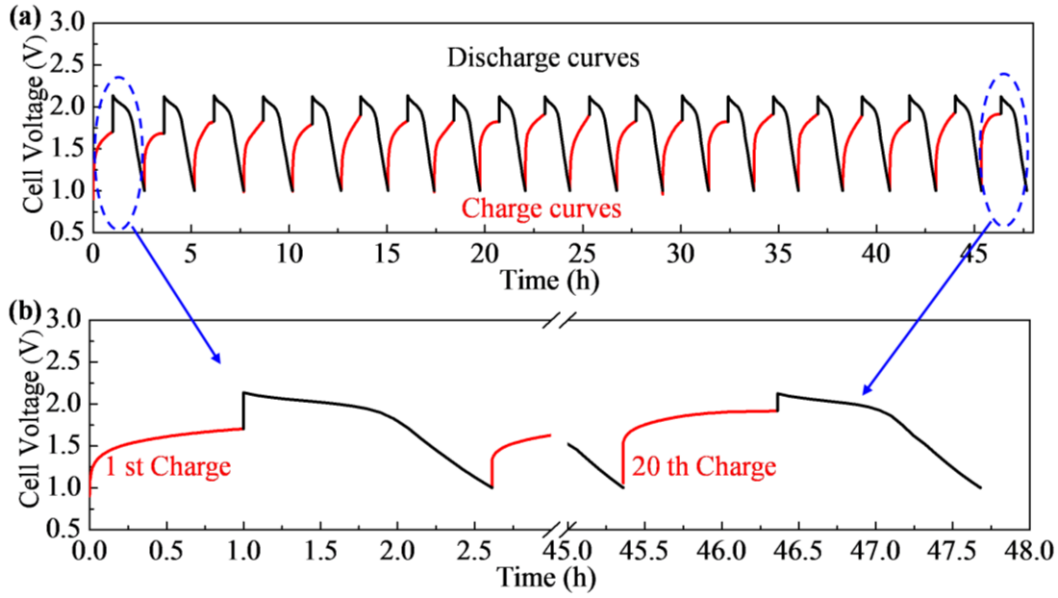

Fig. 3.12 (a,b) Charge curves at a current density of 0.02 mA cm^{-2} and discharging curves at a current density of 0.01 mA cm^{-2} of photoassisted rechargeable SIB under the illumination for 1 h.

The electrochemical properties of photoassisted rechargeable SPIB at a high current density for a long time has been further studied. Fig. 3.13 shows the charge and discharge curves of the photoassisted rechargeable organic SIB at a current density of 0.05 mA cm^{-2} for 4 h. The photoassisted battery still can remain a long charge voltage

plateau at 1.85 V and deliver the discharging capacity of 107 mAh g^{-1}. The performance of photoassisted rechargeable organic SIB can be further improved by combining a flow-through-mode system.

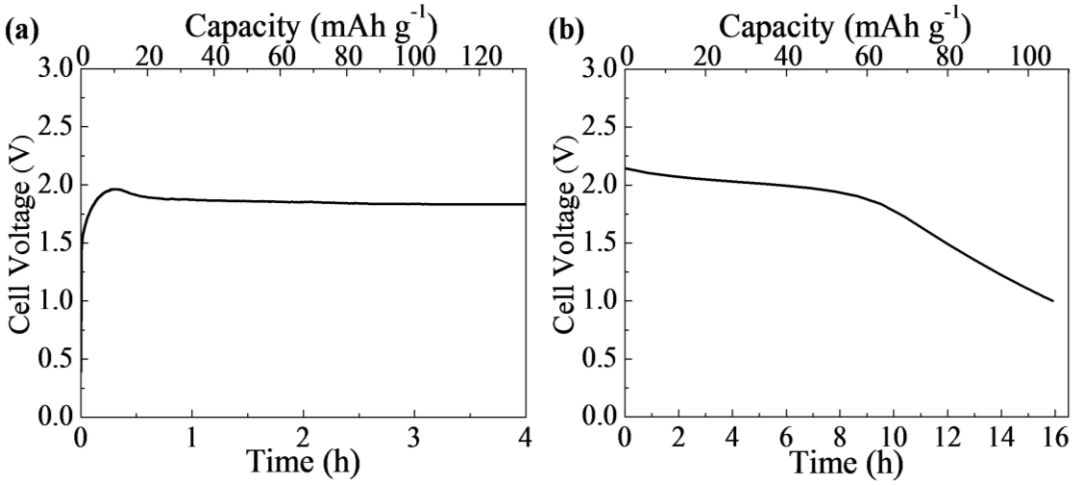

Fig. 3.13 (a) Charge curve of photoassisted rechargeable SIB at a current density of 0.05 mA cm^{-2} and (b) Discharge curve at a current density of 0.01 mA cm^{-2}.

3.4 Conclusions

In summary, we successfully demonstrated the solar energy storage in organic batteries with a photoassisted rechargeable organic SIB as the example. The Ta_3N_4 photoelectrode is advantageous as a photoelectrode due to the visible light absorption, and good stability in organic systems. By utilizing solar energy, the photoassisted rechargeable SIB can be charged at a voltage of 1.65 V, which is lower than its discharging voltage of 2.02 V. The charging voltage reduction translates to energy

saving of ~14% compared to conventional organic SIB. For the first time, we reduce the charging voltage of organic SIB to 1.65 V with the compensate of visible-light. Because it uses the low-cost sodium source and high-voltage I^-/I_3^- redox couples, this photoassisted organic SIB not only works with a higher output voltage but also is more cost-effective. Especially, this concept of internal photoelectrode in organic batteries provides a guiding design for the future large-scale applications of solar energy.

Chapter 4. A photoassisted rechargeable organic/aqueous hybrid battery

4.1 Introduction

The conventional organic/aqueous hybrid batteries combine the advantages of organic and aqueous batteries with the high voltage window and metal anode which has the ultralow voltage. Thus, we have assembled a photoassisted rechargeable hybrid lithium-ion battery (LIB) for photoassisted charging. The conventional rechargeable LIB is one of the indispensable electric energy storage systems with the wide commercialization, and has realized the large-scale application such as the electric vehicles, grid applications etc..[100, 101] The olivine-type $LiFePO_4$ has been reported as a typical cathode material for the LIBs by Padhi et al.[102] Compared to cobalt-based electrode materials, $LiFePO_4$ has the advantages of inherent merits including low toxicity, potential for low cost, long cycle ability and high safety. In especial, this material can be reversibly charged and discharged with a stable voltage profile at 3.45 V vs. Li^+/Li.[103-105] Therefore, integrating TiO_2 into the conventional Li-$LiFePO_4$ battery will represent an important direction for the future application in solar energy conversion and storage.

However, the solid materials are hard to be oxidized by the photoexcited holes generated in the photoelectrode. In this work, a new strategy with the integration of redox couples in the electrolyte has been proposed for photoassisted charging, so that the feasibility of solar energy storage in hybrid battery has been demonstrated in the convention Li-$LiFePO_4$ battery. On account of the photovoltage compensation, the photoassied rechargeable Li-$LiFePO_4$ battery can be charged at a low and stable voltage of 2.78 V for the first time. It is noteworthy that this photoassisted charge

voltage is obviously lower than the 3.41 V discharge voltage. A ~20% electric energy saving has been obtained by the photoassited charging. This idea opens a new avenue for the future application of solar energy conversion and storage in the commercial rechargeable batteries.

4.2 Experiment and characterization

4.2.1 Preparation of photoelectrode

The TiO_2 photoelectrode was prepared by a modified hydrothermal method and sequent heat-treatment. And this photoelectrode was constituted by the TiO_2 nanorod grown on the Ti mesh.[31] During a specific process, the Ti mesh firstly was needed to pretreat in muffle furnace at 500 °C for 10 min. The pretreated Ti mesh was immersed in a 28 ml aqueous solution of 450 μl $TiCl_4$ (99.0%, Sigma-Aldrich) and 1.4 ml HCl (37%, Wako), and sealed in the reaction kettle. Then, the hydrothermal reaction was processed at 170 °C for 10 h. After the hydrothermal treatment, the sample was washed and dried for the next calcination at 450 °C for 2 h. Later, TiO_2 photoelectrode with high crystallinity was obtained.

4.2.2 Assembly of photoassisted rechargeable hybrid battery

As shown in the Fig. 4.1, the photoassisted rechargeable LIB was constructed by a metallic Li anode with organic electrolyte, a LATP glass ceramic separator, a $LiFePO_4$ cathode with aqueous electrolyte, and a TiO_2 photoelectrode. The anode side was prepared in an Ar-filled glove box (<1 p.p.m. of H_2O and O_2). The lithium foil with a thickness of 0.2 mm was cut to a rectangle of 8×40 mm, and then pressed onto a Cu mesh (Nilaco Cor., 100 mesh). An organic electrolyte of 1 M $LiClO_4$ in ethylene carbonate (EC)/dimethyl carbonate (DMC) with a volume ratio 1:1 was added into

this glass cylinder. LATP glass ceramic separator was supplied by Ohara Inc., Japan. The thickness and the electrical conductivity of the LATP plate at 25 °C was 150 μm and 1.05×10^{-4} S cm^{-1}. The LATP was fixed on top of the glass cylinder thus sealing in the anode. The cathode ($LiFePO_4$) and photoelectrode (TiO_2) were stuck on the other cylindrical shape of the quartz shell. An aqueous electrolyte of 0.1 M Li_2SO_4 and 0.01 M LiI was added into this quartz cylinder. The $LiFePO_4$ cathode was prepared by mixing the $LiFePO_4$ with Super P carbon and polytetrafluoroethylene (PTFE) in a weight ratio of 8:1:1. The resulting slurry was then cast on a Ti mesh to achieve a loading of 0.5 mg cm^{-2}.

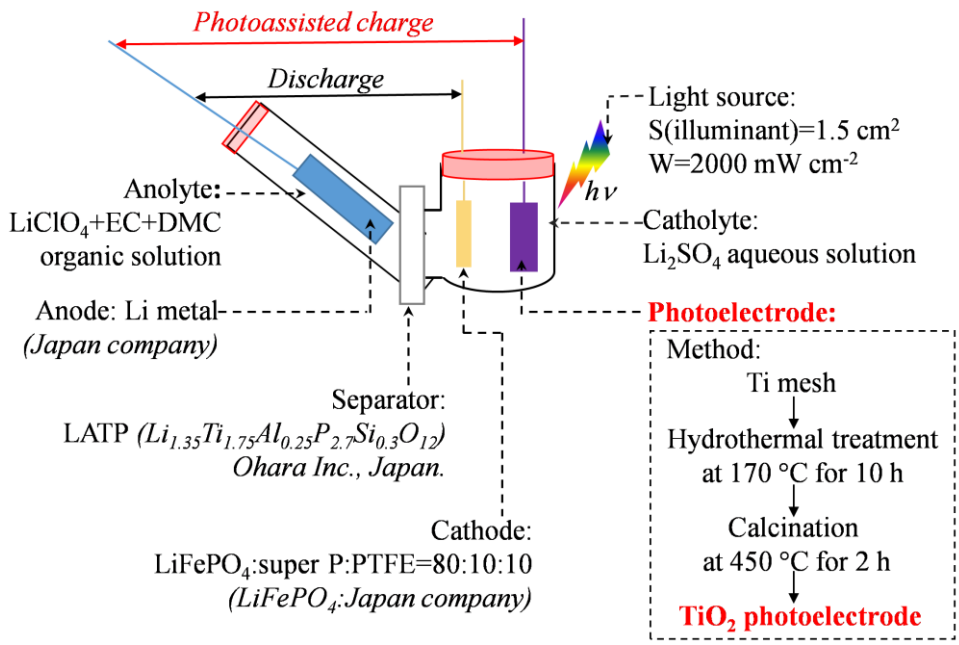

Fig. 4.1 Fabrication of a photoassisted rechargeable hybrid LIB.

4.2.3 Electrochemical and photoelectrochemical measurements

The photoassisted chargeable LIBs were tested using a Hokuto charging/

discharging machine, within a voltage range between 3.1 and 3.7 V, with the discharge/charge current densities varying from 0.02-0.04 mA cm^{-2}. A XEF-501S Xe-lamp (San-ei Electric Co., Japan) was used as the light source. The electrochemical reaction was investigated using CV a Solartron instrument.

4.2.4 Characterizations

XRD was performed using a Bruker D8 Advanced diffractometer with Cu Kα (λ = 1.5406 Å) radiation. The UV-visible absorption spectrum measurements were performed using Shimadzu UV3101PC. SEM observation was performed on a Hitachi S4800.

4.3 Results and discussion

4.3.1 Design of a photoassisted rechargeable hybrid battery

Fig. 4.2 outlines the structure of our photoassisted chargeable LIB. It is constituted by a metal Li anode with organic electrolyte, a $Li_{1.35}Ti_{1.75}Al_{0.25}P_{2.7}Si_{0.3}O_{12}$ (LATP) glass ceramic separator, a $LiFePO_4$ cathode with aqueous electrolyte, and a TiO_2 photoelectrode. In the cathode side, a redox couple (M) has been integrated into a high safe and low-cost aqueous system for contacting the $LiFePO_4$ and TiO_2 photoelectrode. At the same time, the aqueous system also can reduce the heating effect during a long-term illumination. During the charging under illumination, a photoassisted charging voltage is performed on the anode Li and TiO_2 photoelectrode, and an oxidation reaction occurs on the photoelectrode firstly. That is, the photoexcited holes on TiO_2 photoelectrode can oxidize M^{red} into M^{ox}. Subsequently, the M^{ox} diffuses to the $LiFePO_4$ solid electrode surface and oxidizes $LiFePO_4$ to

$FePO_4$ and Li^+. In this process, M^{ox} is reduced to M^{red}, so that a redox process has been completed. Meanwhile, the photoexcited electron transfers to the anode through the external circuit, where it then reduces the Li^+ ion to Li metal. The equations of photoassited charge and discharge are as follows:

Photoassisted charge: $h\nu \rightarrow TiO_2 \rightarrow h^+ + e^-$ (photoelectrode)

$2h^+ + 3I^- \rightarrow I_3^-$ (catholyte)

$I_3^- + 2LiFePO_4 \rightarrow 2FePO_4 + 3I^- + 2Li^+$ (cathode)

$Li^+ + e^- \rightarrow Li$ (anode)

Discharge: $Li^+ + FePO_4 + e^- \rightarrow LiFePO_4$ (cathode)

$Li \rightarrow Li^+ + e^-$ (anode)

As presented in Fig. 4.2b, the photoassisted charging potential equals the energy difference between the redox potential of the Li^+/Li couple and the quasi-Fermi level of the electrons in the TiO_2 photoelectrode (which is near to the conduction band CB of the TiO_2).

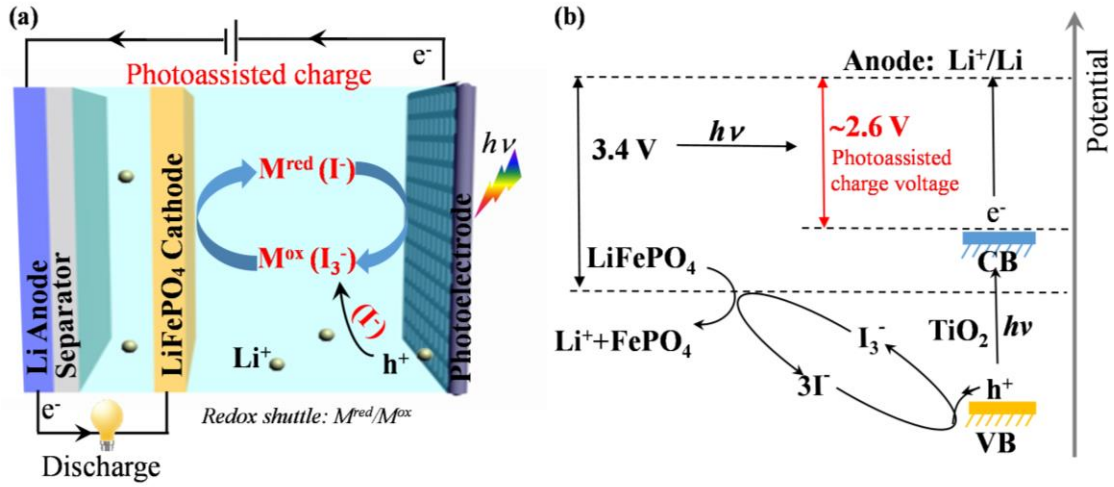

Fig. 4.2 (a) Schematic of a photoassisted rechargeable hybrid LIB. (b) Potential diagram for the photoassisted charging process. The photoassited charge voltage is

determined by the energy difference between anode voltage of LIB and quasi-Fermi level of electrons in the TiO_2 photoelectrode (near to its conduction band (CB)).

Since the CB potential of TiO_2 (～2.6 V)[106, 107] is lower than the $LiFePO_4/FePO_4$ standard potential of ～3.45 V, the photocharging voltage is expected to be lower than that of conventional Li-$LiFePO_4$ batteries.

The photoelectrode was rutile-phase TiO_2 nanorods grown on a Ti mesh, the morphology and crystal structure were investigated by scanning electron microscopy (SEM) (Fig. 4.3a) and X-ray diffraction (XRD) analysis (Fig. 4.3b). The open structure, as revealed in the SEM images, allows the free diffusion of I^-/I_3^- ions in the electrolyte between the photoelectrode and the $LiFePO_4$ cathode.

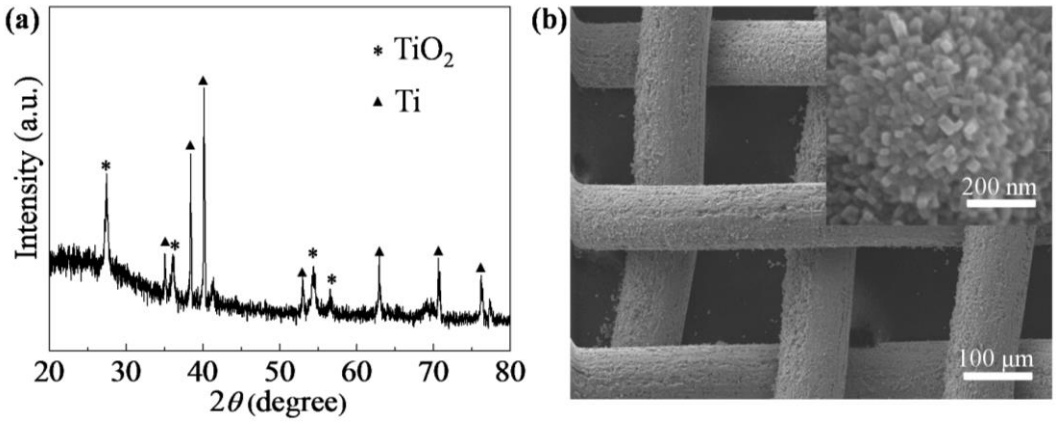

Fig. 4.3 XRD pattern (a) and SEM images (b) of the TiO_2 photoelectrode (b high-magnification SEM image is shown as the inset).

4.3.2 Electrochemical performance without illumination

Firstly, the electrochemical performance of the LIB containing a metal Li anode

with organic electrolyte, a LATP separator, and a $LiFePO_4$ cathode with aqueous electrolyte has been investigated without illumination. It can be seen that an average charging voltage of 3.45 V and discharging voltage of 3.41 V (Fig. 4.4a), consistent with the reported redox potential of $LiFPO_4/FePO_4$ in aqueous electrolyte.[108, 109] The charging and discharging capacity are 149 and 138 mAh g^{-1}, respectively. The CV measurement between 3.1 and 4.0 V (Fig. 4.4b) reveals that the aqueous cathode is electrochemically stable evidenced by neither H_2 nor O_2 evolution. We then consider the chemical delithiation process of $LiFePO_4$ by I_3^- ions. The cyclic voltammetry (CV) reveals that the potential of I^-/I_3^- redox couple is about 3.55 V (Fig. 4.4b), consistent with earlier study,[110] higher than the $LiFePO_4/FePO_4$ standard potential of ~3.45 V. Hence, the oxidization of $LiFePO_4$ by I_3^- is thermodynamically feasible with a driving potential of 0.1 V.

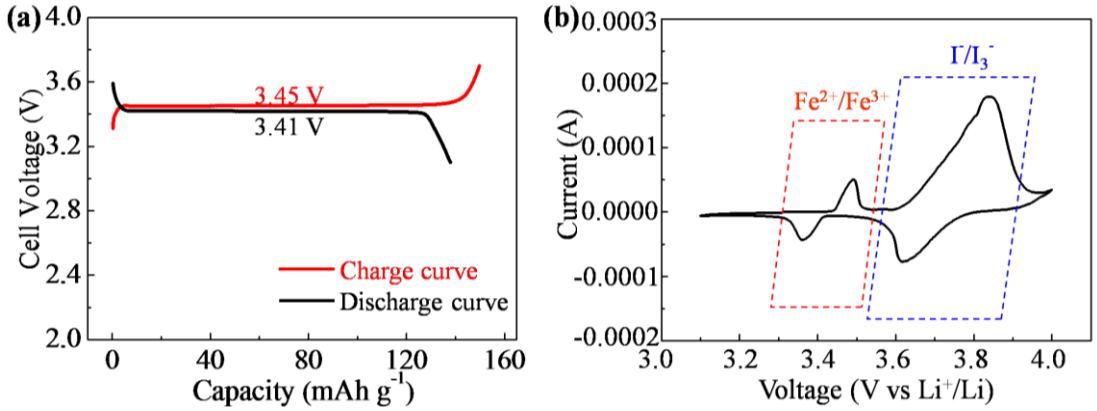

Fig. 4.4 Charge and discharge curves (a) of Li-ion battery at a current density of 0.01 mA cm^{-2}. (b) CV curve of Li-ion battery in the 1 M Li_2SO_4 and 0.01 M LiI aqueous solution at a scan rate of 0.01 mV s^{-1}.

4.3.3 Feasibility analysis of photoassisted charge

A suitable redox shuttle is the key component of the photoassisted chargeable LIB, which has to fulfill two essential conditions: 1) M^{red} should be oxidized to M^{ox} by photoexcited holes on the TiO_2 photoelectrode. 2) M^{ox} should enable the chemical oxidization from $LiFePO_4$ to $FePO_4$ and Li^+ ion. Here, we considere I^- ions as the redox shuttle for our system, and it is essential to confirm that I^- ions will work efficiently. Despite that I^-/I_3^- ions are used as a traditional redox shuttle for DSSC,[111-113] not much attention is paid to the combination of TiO_2 photoelectrode and I^-/I_3^- ions in aqueous electrolyte. Therefore, we started with investigating this photo- electrochemical oxidation reaction.

To investigate interaction between I^- ions and the TiO_2 photoelectrode, an aqueous solution of 0.05 M I^- ions with the TiO_2 photoelectrode was analyzed by the ultraviolet-visible (UV-Vis) spectra after 1 h illumination. As shown in Fig. 4.5a, two peaks attributed to I_3^- ions (288 and 350 nm) were identified, proving the feasible photoelectrochemical oxidation reaction from I^- to I_3^- ions aided by the TiO_2 photoelectrode. The chemical delithiation reaction was examined by monitoring the crystal structure changes of $LiFePO_4$ in I_3^- aqueous solution. After soaking the $LiFePO_4$ powers in an aqueous solution of 0.1 M I_3^- ion for 10 min, the crystal structure of $LiFePO_4$ completely transformed into that of $FePO_4$ (Fig. 4.5b), indicating that the I_3^- ions can rapidly oxidize $LiFePO_4$ into $FePO_4$ in a very short time. Based on above results, the I^-/I_3^- ions can be used as the redox shuttle for the photoelectrochemical oxidation reaction (Equations 1, 2) and the chemical delithiation of $LiFePO_4$ (Equation 3) during the photocharging process, described as the following Equations:

$$TiO_2 + h\nu \rightarrow h^+ + e^- \quad (1)$$

$$2h^+ + 3I^- \rightarrow I_3^- \quad (2)$$

$$I_3^- + 2LiFePO_4 \rightarrow 2FePO_4 + 3I^- + 2Li^+ \quad (3)$$

The charging and discharging curves of the photoassisted rechargeable LIB and LIB are shown in Fig.4.6. Under illumination, the photoassisted rechargeable LIB delivers a charging voltage of 2.78 V at a current of 0.02 mA cm^{-2}, which matches well with the theoretical prediction, considering the CB potential of TiO_2 (～2.6 V). Compared to the LIB, which has a charging voltage of 3.45 V, the photoassisted rechargeable LIB achieves a voltage reduction of 0.7 V, resulting in energy saving of 20% (0.7/3.45 ×100%). After 3 h photocharging process, our photoassisted rechargeable LIB delivers a long discharge voltage plateau at about 3.41 V and a discharge capacity of 104 mAh g^{-1} at a current of 0.01 mA cm^{-2}, which is similar with that of the LIB (Fig. 4.6b). It is noticeable that this charging voltage is lower than the discharging voltage, which is thermodynamically impossible without the solar energy input.

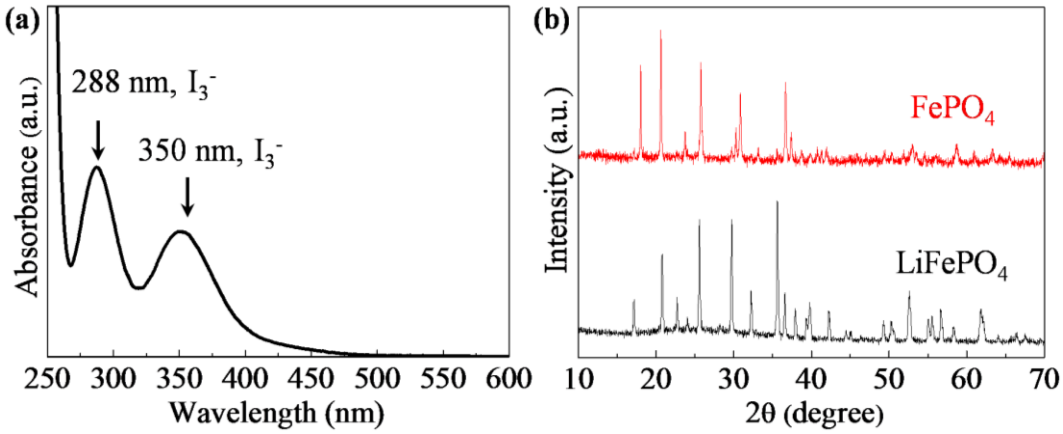

Fig. 4.5 (a) UV-Vis spectrum of 0.05 M I^- ions solution containing TiO_2 photoelectrode after 1 h illumination. (d) XRD patterns of the $LiFePO_4$ (black line) and the product (red line) prepared by placing 50 mg $LiFePO_4$ in an aqueous solution of 0.1 M I_3^- for 10 min.

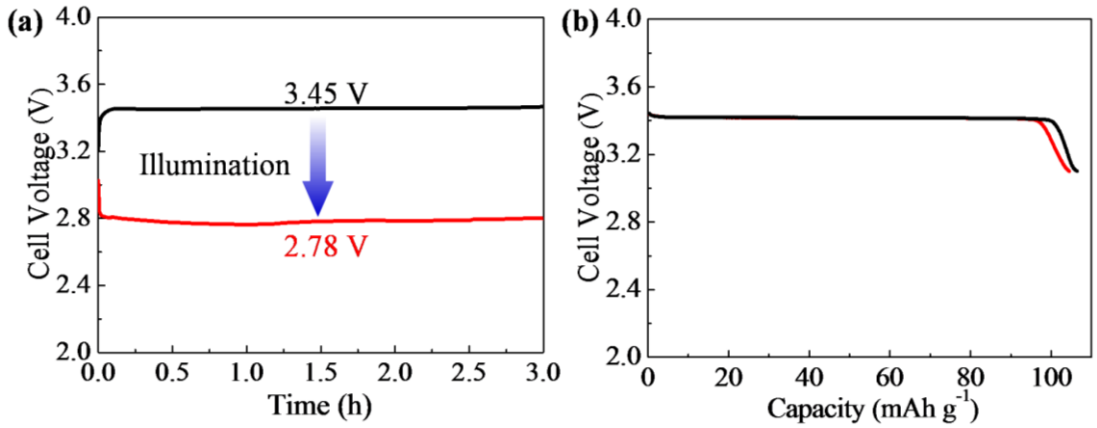

Fig. 4.6 (a) Charge curves of photoassisted rechargeable LIB (red line) and LIB (black line) at a current density of 0.02 mA cm^{-2}. (b) Corresponding discharge curves at a current density of 0.01 mA cm^{-2}.

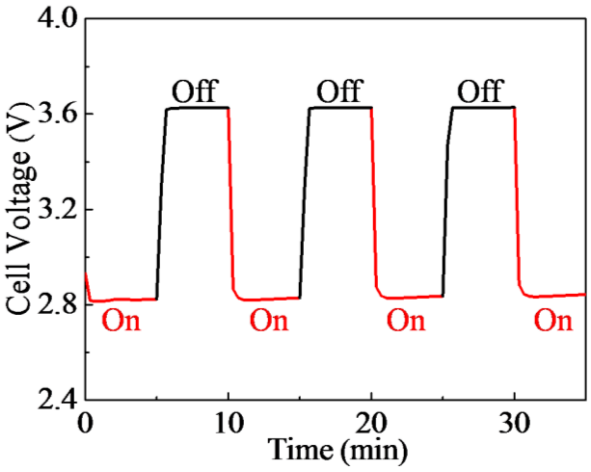

Fig. 4.7 Light-response of the charge voltage of a photoassisted rechargeable LIB when illumination was switched from “on” to “off”.

For the light-response of the photoassisted rechargeable LIB, once the illumination was removed, the charging voltage was increased to 3.62 V immediately, and this phenomenon is observed to be consistent and repeatable at least in three repeat cycles (Fig. 4.7). Such a fast photo-response behavior effectively demonstrates our proposed working mechanism of the photoassisted charging.

4.3.4 Photoassisted electrochemical performance

The charging/discharging curves of the photoassisted chargeable LIB at current rates from 0.02 to 0.04 mA cm^{-2} have been shown in Fig. 4.8. It is notable that the degree of polarization does not drastically increase. The photoassisted charging voltage is recorded as 2.88 V, even at the current of 0.04 mA cm^{-2}. The discharging capacity increased to 137 mAh g^{-1} after photocharging for 3 h at the current of 0.04 mA cm^{-2}.

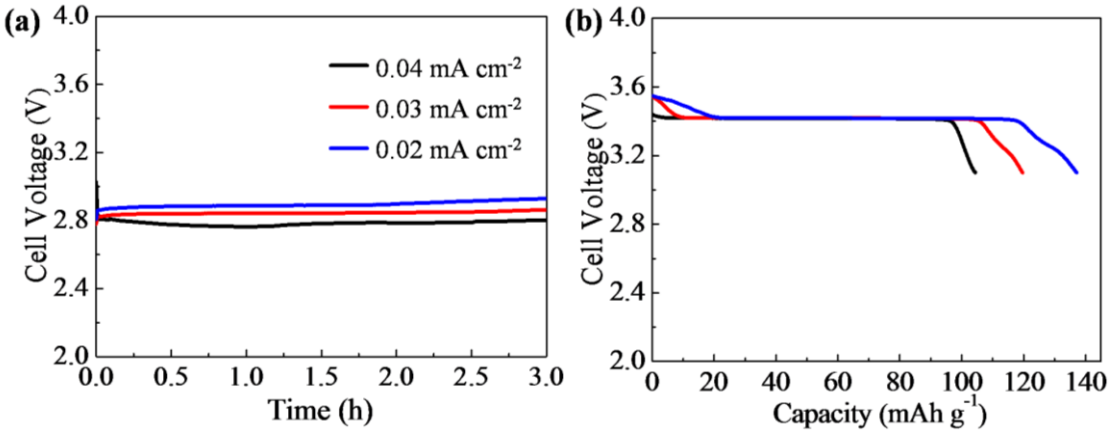

Fig. 4.8 (a) Charge curves of photoassisted rechargeable LIB at different currents. (b) Corresponding discharge curves at a current density of 0.01 mA cm^{-2}.

In order to evaluate the stability of the photoassisted chargeable LIB, the cycling performances of the photoassisted chargeable LIB after 3 h and 1 h illumination have been studied respectively. Reversible cycling was observed for 10 cycles without notable change in the charging voltage (Fig. 4.9), suggesting the excellent stability of the device. After 10 cycles, the discharge capacity retention of the battery is about 93% for 3 h illumination and 107% for 1h illumination, respectively. Interestingly, it can be observed that the discharge capacity after 1 h illumination increased during the 10 cycles (Fig. 4.9b), suggesting a possible activating process in the photocatalyst.

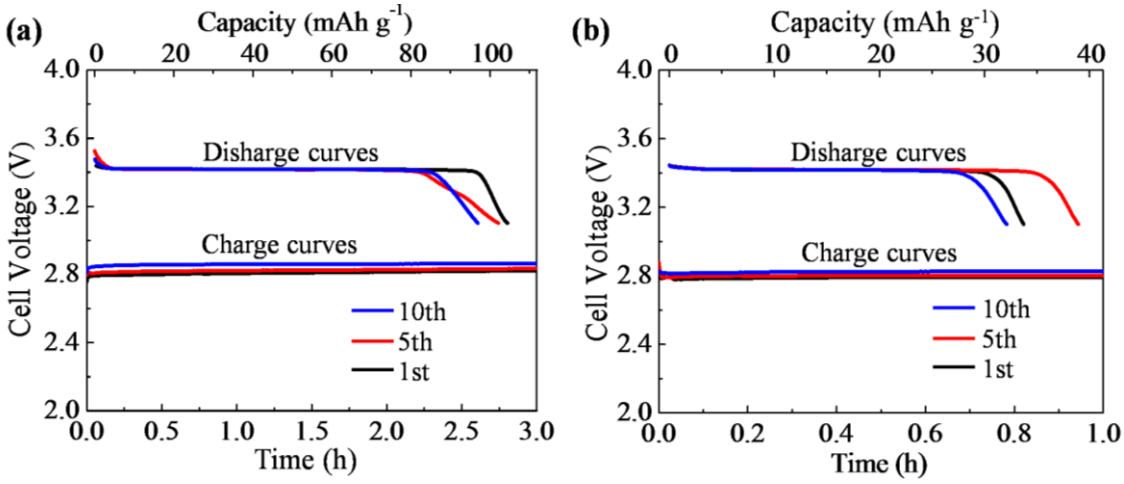

Fig. 4.9 Charge curves at a current of 0.02 mA cm^{-2} and discharge curves at a current density of 0.01 mA cm^{-2} of photoassisted rechargeable LIB under the illumination for 3 h (a) and 1 h (b).

The comparison diagrams of charge voltage and maximum energy conversion efficiency of photoassisted rechargeable LIB and LIB are shown in Fig. 4.10. After the illumination for 3 h, the photoassisted rechargeable LIB could deliver a ~113% energy conversion efficiency (output electric energy/input electric energy), which is

obviously higher than ~92.6% of conventional LIB. In addition, it is worth pointing out that the energy conversion efficiency of the photoassisted rechargeable battery after 1 h illumination is 121%, significantly higher than that of LIB (that is, 96.5%), attributing to the reduced voltage during photocharging process.

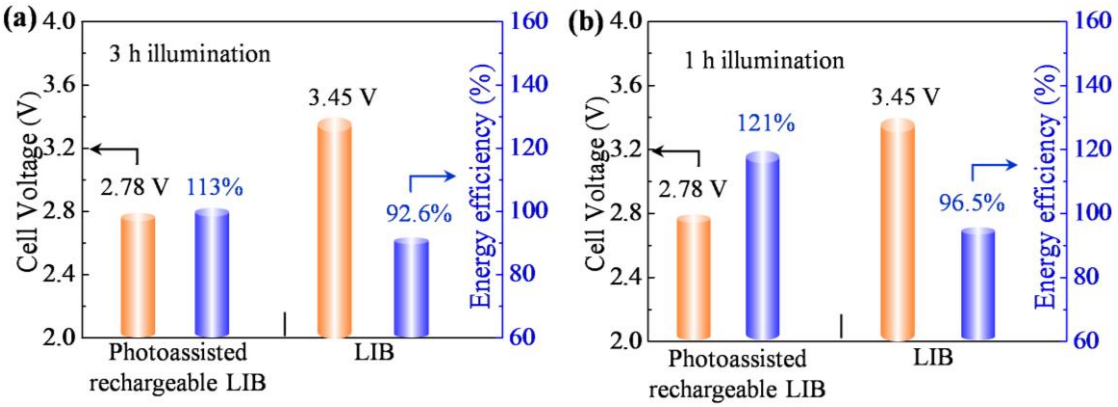

Fig. 4.10 Comparison diagrams (a, b) of charge voltage and maximum energy conversion efficiency of photoassisted rechargeable LIB and LIB.

4.4 Conclusions

In summary, the feasibility of solar energy conversion/storage in rechargeable hybrid battery has been demonstrated by proposing a novel photoassisted rechargeable LIB, which can capture and store solar energy into a conventional LIB without the external combination of PVs. This battery is constituted by a lithium anode, a $LiFePO_4$ cathode, and a TiO_2 photoelectrode with I^-/I_3^- ions redox couples. On the photoassisted charging, the photoexcited holes on TiO_2 photoelectrode enable to oxidize the I^- into I_3^-, then the I_3^- oxidizes the $LiFePO_4$ into $FePO_4$ and I_3^- can be reduced to I^- in the cathode side by the chemical process. Besides, the photoexcited

electrons on TiO_2 photoelectrode can transfer to anode side with the reduction of Li^+ ion into Li metal. The generated photovoltage is utilized to compensate the required charging voltage. Through the utilization of solar energy, a charging voltage of 2.78 V has been obtained for the photoassisted rechargeable LIB, and this value is lower than the discharging voltage of 3.41 V. With the comparison with conventional LIB, the reduction of charging voltage results in saving the ~20% input electric energy. Thus, the charging voltage of the $LiFePO_4$ cathode is firstly reduced to 2.78 V by introducing a photoelectrode with redox shuttle into the LIB. With the incorporation of the appropriate redox couples, the photoassisted charging strategy could be utilized into other solid electrode materials.

Chapter 5 Conclusions

In this research, to realize the conversion and storage of free and abundant solar energy into the rechargeable batteries, we designed the three-types photoassisted rechargeable batteries and made a series of investigation for the feasibility and photoassisted electrochemical performance. Main conclusions are shown as follows:

In Chapter 2, the solar energy has simultaneously converted and stored into an aqueous SPIB through a photoassisted charging strategy. The photoassisted rechargeable aqueous SPIB employs the aqueous anolyte and catholyte, and a TiO_2 photoelectrode integrated into the catholyte for capturing solar energy. Due to the compensation of photovoltage, an ultralow charging voltage of 0.08 V is achieved, which is lower than its discharging voltage of 0.83 V. The charging voltage reduction results in saving ~90% input electric energy.

In Chapter 3, a Ta_3N_5 as a visible light-driven photocatalyst has been integrated into a full organic SIB for realizing the conversion and storage of the wider solar energy. The assembled photoassisted chargeable SIB employs P2-$Na_{0.66}Ni_{0.17}Co_{0.17}Ti_{0.66}O_2$ and NaI as the active materials of anode and cathode respectively. Under the visible light, a low charging voltage of 1.65 V is achieved, which is lower than its discharging voltage of 2.02 V. The charging voltage reduction results in the ~14% input electric energy saving.

In Chapter 4, a photoassisted rechargeable hybrid LIB has been proposed and it enables to capture and store solar energy into the conventional LIB by a TiO_2 photoelectrode. Through utilizing solar energy, the photoassisted rechargeable LIB can be charged at a voltage of 2.78 V, which is lower than its discharging voltage of 3.41 V. The charging voltage reduction translates to energy saving of ~20% compared to conventional LIB.

Table 5.1 Summary of the three-types photoassisted rechargeable batteries in this research.

Type	Photo electrode	Active materials in anode/cathode	Separator	Discharge voltage	Capacity	Cycling numbers	η_1
Aqueous	TiO_2	Na_2S_4/NaI	Nafion	0.83 V	110 mAh g^{-1}	20 cycles (0.08→0.11V)*	90%
Organic	Ta_3N_5	$Na_{0.66}Ni_{0.17}Co_{0.17}Ti_{0.66}O_2$ /NaI	PNP	2.02 V	107 mAh g^{-1}	20 cycles (1.65→1.78V)*	14%
Hybrid	TiO_2	Li/$LiFePO_4$	LATP	3.41 V	137 mAh g^{-1}	10 cycles (2.78→2.86 V)*	20%

*η_1: Saving input electric energy, *: photoassisted charging voltage.*

Based on the detailed researches and the summary on electrochemical performance in the Table 5.1, a comprehensive comparison for three-types photoassisted rechargeable batteries has been taken from the characteristics and applications as follows:

1) Characteristics of the three-types photoassisted rechargeable batteries.

Firstly, the photoassisted rechargeable aqueous SPIB employs the anolyte and catholyte as the active materials in anode and cathode, and the TiO_2 photoelectrode in the specific aqueous-system displays a fast light-response and the stable and low charging voltage. While, to avoid the electrolysis of water, the photoassisted rechargeable aqueous battery presents the limited voltage window and discharge voltage. Secondly, the photoassisted rechargeable organic SIB respectively employs the safe $Na_{0.66}Ni_{0.17}Co_{0.17}Ti_{0.66}O_2$ and the high-voltage NaI as the active materials in anode and cathode, and the typical organic system make this-type photoassisted rechargeable battery display a wide voltage window and the high discharging voltage.

In particular, the designed battery enables to charge by the visible-light driven due to the integration of Ta_3N_5 photoelectrode. While this photoelectrode in this organic system shows a slower light-response. Thirdly, the photoassisted rechargeable organic/aqueous hybrid LIB combines the advantages of aqueous and organic batteries by employing low-voltage Li and the commercial $LiFePO_4$ as the active materials in anode and cathode. The battery displays the wide voltage window and the high discharge voltage, simultaneously the integration of TiO_2 photoelectrode in an aqueous cathode takes the battery show a fast light-response.

2) Applications of the three-types photoassisted rechargeable batteries.

Due to the compensation of solar energy, the three-types photoassisted rechargeable batteries all have shown the application potential in the photoassisted charging of daytime, and enable to charge by the extra electric energy input at night. However, the various electrochemical performances and systems make the photoassisted rechargeable batteries display different potential applications. Firstly, the photoassisted rechargeable aqueous SPIB with the flowable aqueous system could be applied in the modular and low-cost electric devises with the limited voltage requirements. Secondly, the photoassisted rechargeable organic SIB could be applied into some electric devises with the requirements of high voltage and high security. Thirdly, the photoassisted rechargeable hybrid LIB shows the great utilization potentiality in some electric devises with the high-voltage and fast light-response demand.

Although our research has simultaneously converted and stored the solar energy into the multiple rechargeable batteries by a photoassisted charging strategy, and realized the efficient saving of electric energy, much effort should further be devoted to realizing the practical applications of solar energy in the electric energy devices.

List of research results

JOURNAL PAPER

First-author related to this Ph.D. thesis

[1] Qi Li, Na Li, Yang Liu, Yarong Wang, Haoshen Zhou, High-safety and low-cost photoassisted chargeable aqueous sodium-ion batteries with 90% input electric energy savings, Advanced Energy Materials, 2016, 6, 1600632.

[2] Qi Li, Na Li, Masayoshi Ishida, Haoshen Zhou, Saving electric energy by integrating a photoelectrode into a Li-ion battery, Journal of Materials Chemistry A, 2015, 3, 20903.

[3] Qi Li, Yang Liu, Shaohua Guo, Haoshen Zhou, Solar energy storage in the rechargeable batteries, Nano Today, 2017, Submitted.

[4] Qi Li, Yang Liu, Shaohua Guo, Haoshen Zhou, Solar energy storage in the organic sodium ion battery by the visible-light driven, in preparation.

Other publications

[1] Qi Li, Shaohua Guo, Kai Zhu, Kezhu Jiang, Xiaoyu Zhang, Ping He, Haoshen Zhou, A post-spinel anode enabling sodium-ion ultralong cycling and superfast transport via 1D channels, Advanced Energy Materials, 2017, 1700361.

[2] Shaohua Guo, Qi Li, Pan Liu, Mingwei Chen, Haoshen Zhou, Environmentally stable interface of layered oxide cathodes for sodium-ion batteries, Nature Communications, 2017, DOI: 10.1038/s41467-017-00157-8.

[3] Yang Liu, Na Li, Kaiming Liao, Qi Li, Masayoshi Ishida, Haoshen Zhou, Lowering the charge voltage of Li–O_2 batteries via an unmediated photoelectrochemical

oxidation approach, Journal of Materials Chemistry A, 2016, 4, 12411.

PRESENTATION

[1] Qi Li, Haoshen Zhou, Integrating a photoelectrode into a Li-ion battery for saving electric energy, 2016 International Conference on Green Energy and Applications, Singapore, March 23-24, 2016 (oral).

Acknowledgements

Precious time goes fast! Unconsciously, the three-year course of doctoral candidate is coming to end. Looking back over the past, I feel very excited for the achieved development in the study and life. In this very special moment, I would like to express my sincere gratitude to all those who have given me generous help on my way.

First and foremost, I would like to express deepest gratitude to my supervisor Professor Haoshen Zhou (professor at University of Tsukuba and principle investigator at AIST). Thanks for his constant encouragement and guidance. He has walked me through all the stages of the doctoral study. Without his thoughtful and thorough guidance, and insightful criticism, this thesis could not have reached its present form. He instructed me study that how to proceed research with perseverance, and I have benefited a lot from his scientific spirit. He always had many innovative ideas and inspired me to make better work.

I also express my heartfelt gratitude to vice-supervisors Prof. Masayoshi Ishida, Associate Prof. Nobuko Hanada, and Associate Prof. Hirohisa Aki at University of Tsukuba. When I entered the university, Ishida sensei, Hanada sensei and Aki sensei gave their selfless assistance in my study and life. In particular, I feel sincerely grateful to the instruments of Prof. Masayoshi Ishida, Prof. Keiichi Okajima, Associate Prof. Hirohisa Aki and Dr. Eunjoo Yoo in the graduation presentation, their very valuable suggestions and ideas deeply inspired me.

I greatly thank the help of Dr. Na Li and Dr. Shaohua Guo. Dr. Na Li gave much suggestions and useful discussions on the research of solar energy storage in rechargeable batteries, and encouraged me to persistently research on this new field. I will keep on my special thanks to Dr. Shaohua Guo, who helped me start my initial experimental researches on sodium-ion batteries and made progress in my research

work.

Many thanks are wished to give to all the group members in the Energy Interface Technology Research Group at AIST. Dr. Hirofumi Matsuda, Dr. Eunjoo Yoo, Dr. Hirokazu Kitaura and Mr. Jun Okagaki, gave me their kind help in the entire doctoral research. I also would like to express my gratitude to Dr. Xizheng Liu, Dr. Kaiming Liao, Dr. Yang Sun, Dr. Jin Yi, Dr. Yarong Wang, Dr. Kai Zhu, Mr. Yu Qiao, Mr. Xiang Li and Ms. Yibo He for their kindly help in my doctoral research and life. Furthermore, my sincerely gratitude goes to my classmates, Dr. Shichao Wu, Dr. Sunyan Bai, and Ms. Yang Liu. We all came to the University of Tsukuba in 2014, and started to discuss together about the research and achieved lots of improvements.

I would like to express my thanks to the financial support provided by the China Scholarship Council. It ensured that I could focus on the research work.

Finally, I am extremely grateful for my father Haiyi Li, mother Yanping Li, little brother Lianjie Li and boyfriend Longhai Yang. Their loving considerations and great confidence will inspire me all through these years and future life.

REFERENCE

[1] R. Perez, K. Zweibel and T. E. Hoff, Solar power generation in the US: too expensive, or a bargain? Energy Policy 39: 7290-7297, 2011.

[2] S. Chu and A. Majumdar, Opportunities and challenges for a sustainable energy future, Nature 488: 294-303, 2012.

[3] A. G. Griesbeck, J. Steinwascher, M. Reckenthaler and J. Uhlig, Azide/oxygen photocatalysis with homogeneous and heterogeneous photocatalysts for 1,2-aminohydroxylation of acyclic/cyclic alkenes and michael acceptors, Res. Chem. Intermediat. 39: 33-42, 2013.

[4] K. Ohkubo, T. Kobayashi and S. Fukuzumi, Direct oxygenation of benzene to phenol using quinolinium ions as homogeneous photocatalysts, Angew. Chem. Int. Ed. 50: 8652-8655, 2011.

[5] S. Fukuzumi, S. Kato and T. Suenobu, Combination of visible-light responsive heterogeneous and homogeneous photocatalysts for water oxidation, Phys. Chem. Chem. Phys. 13: 17960-17963, 2011.

[6] J. Zhao, X. Wang, Z. Xu and J. S. C. Loo, Hybrid catalysts for photoelectrochemical reduction of carbon dioxide: a prospective review on semiconductor/metal complex co-catalyst systems, J. Mater. Chem. A 2: 15228, 2014.

[7] A. Fujishima and K. Honda, Photolysis-decomposition of water at the surface of an irradiated semiconductor, Nature 238: 37-38, 1972.

[8] X. Zong, C. Sun, H. Yu, Z. G. Chen, Z. Xing, D. Ye, G. Q. Lu, X. Li and L. Wang, Activation of photocatalytic water oxidation on n-doped zno bundle-like nanoparticles under visible light, J. Phys. Chem. C 117: 4937-4942, 2013.

[9] S. Ouyang, P. Li, H. Xu, H. Tong, L. Liu and J. Ye, Bifunctional-nanotemplate assisted synthesis of nanoporous $SrTiO_3$ photocatalysts toward efficient degradation of

organic pollutant, ACS Appl. Mater. Interfaces 6: 22726-22732, 2014.

[10] Y. Gui, Y. Cao, G. Li, X. Ai, X. Gao and H. Yang, A solar storable fuel cell with efficient photo-degradation of organic waste for direct electricity generation, Energy Storage Materials 5: 165-170, 2016.

[11] A. Landman, H. Dotan, G. E. Shter, M. Wullenkord, A. Houaijia, A. Maljusch, G. S. Grader and A. Rothschild, Photoelectrochemical water splitting in separate oxygen and hydrogen cells, Nature Mater.16: 646-651, 2017.

[12] H. Tong, S. Ouyang, Y. Bi, N. Umezawa, M. Oshikiri and J. Ye, Nano-photocatalytic materials: possibilities and challenges, Adv. Mater. 24: 229-251, 2012.

[13] H. Kato, K. Asakura and A. Kudo, Highly efficient water splitting into H_2 and O_2 over lanthanum-doped $NaTaO_3$ photocatalysts with high crystallinity and surface nanostructure, J. Am. Chem. Soc. 125: 3082-3089, 2003.

[14] Z. G. Yi, J. H. Ye, N. Kikugawa, T. Kako, S. X. Ouyang, H. Stuart-Williams, H. Yang, J. Y. Cao, W. J. Luo, Z. S. Li, Y. Liu and R. L. Withers, An orthophosphate semiconductor with photooxidation properties under visible-light irradiation, Nature Mater. 9: 559-564, 2010.

[15] B. Luo, G. Liu and L. Wang, Recent advances in 2d materials for photocatalysis, Nanoscale 8: 6904-6920, 2016.

[16] G. Liu, L. Wang, H. G. Yang, H.-M. Cheng and G. Q. Lu, Titania-based photocatalysts-crystal growth, doping and heterostructuring, J. Mater. Chem. 20: 831-843, 2010.

[17] X. Meng, L. Liu, S. Ouyang, H. Xu, D. Wang, N. Zhao and J. Ye, Nanometals for solar-to-chemical energy conversion: from semiconductor-based photocatalysis to plasmon-mediated photocatalysis and photo-thermocatalysis, Adv. Mater. 28: 6781-6803, 2016.

[18] D. M. Robinson, Y. B. Go, M. Greenblatt and G. C. Dismukes, Water oxidation by λ-MnO_2: catalysis by the cubical Mn_4O_4 subcluster obtained by delithiation of spinel $LiMn_2O_4$, J. Am. Chem. Soc. 132: 11467-11469, 2010.

[19] G. P. Gardner, Y. B. Go, D. M. Robinson, P. F. Smith, J. Hadermann, A. Abakumov, M. Greenblatt and G. C. Dismukes, Structural requirements in lithium cobalt oxides for the catalytic oxidation of water, Angew. Chem. Int. Ed. 51: 1616-1619, 2012.

[20] M. Gong, Y. G. Li, H. L. Wang, Y. Y. Liang, J. Z. Wu, J. G. Zhou, J. Wang, T. Regier, F. Wei and H. J. Dai, An advanced Ni-Fe layered double hydroxide electrocatalyst for water oxidation, J. Am. Chem. Soc. 135: 8452-8455, 2013.

[21] P. Niu, L. Zhang, G. Liu and H.-M. Cheng, Graphene-like carbon nitride nanosheets for improved photocatalytic activities, Adv. Funct. Mater. 22: 4763-4770, 2012.

[22] G. Liu, X. Meng, H. Zhang, G. Zhao, H. Pang, T. Wang, P. Li, T. Kako and J. Ye, Elemental boron for efficient carbon dioxide reduction under light irradiation, Angew. Chem. Int. Ed. 56: 5632, 2017.

[23] D. J. Martin, G. Liu, S. J. Moniz, Y. Bi, A. M. Beale, J. Ye and J. Tang, Efficient visible driven photocatalyst, silver phosphate: performance, understanding and perspective, Chem. Soc. Rev. 44: 7808-7828, 2015.

[24] S. Mathew, A. Yella, P. Gao, R. Humphry-Baker, B. F. E. Curchod, N. Ashari-Astani, I. Tavernelli, U. Rothlisberger, M. K. Nazeeruddin and M. Gratzel, Dye-sensitized solar cells with 13% efficiency achieved through the molecular engineering of porphyrin sensitizers, Nature Chem. 6: 242-247, 2014.

[25] A. Gurung, H. Elbohy, D. Khatiwada, A. Mitul and Q. Q. Qiao, A simple cost-effective approach to enhance performance of bifacial dye-sensitized solar cells, IEEE J. Photovolt. 6: 912-917, 2016.

[26] X. Li, D. Q. Bi, C. Y. Yi, J. D. Decoppet, J. S. Luo, S. M. Zakeeruddin, A. Hagfeldt

and M. Gratzel, A vacuum flash-assisted solution process for high-efficiency large-area perovskite solar cells, Science 353: 58-62, 2016.

[27] A. Yella, H. W. Lee, H. N. Tsao, C. Y. Yi and A. K. Chandiran, Porphyrin-sensitized solar cells with cobalt (II/III)-based redox electrolyte exceed 12 percent efficiency, Science 334: 1203-1203, 2011.

[28] M. A. Green, A. Ho-Baillie and H. J. Snaith, The emergence of perovskite solar cells, Nat. Photon. 8: 506-514, 2014.

[29] J. Zhao and X. Yang, Photocatalytic oxidation for indoor air purification: a literature review, Build. Environ. 38: 645-654, 2003.

[30] X. Yue, R. Zhang, H. Wang and F. Zhang, Sorption and decomposition of crude oil using exfoliated graphite/ZnO composites, J. Phys. Chem. Solids 70: 1391-1394, 2009.

[31] X. Wang, W. Wang, X. Wang, J. Zhao, J. Zhang and J. Song, Insight into visible light-driven photocatalytic degradation of diesel oil by doped TiO_2-PS floating composites, Environ. Sci. Pollut. R. 23: 18145-18153, 2016.

[32] K. M. Lee, C. W. Lai, K. S. Ngai and J. C. Juan, Recent developments of zinc oxide based photocatalyst in water treatment technology: a review, Water Res. 88: 428-448, 2016.

[33] S. W. Boettcher, T. E. Mallouk and F. E. Osterloh, Themed issue on water splitting and photocatalysis, J. Mater. Chem. A 4: 2764-2765, 2016.

[34] J. B. Goodenough. Changing outlook for rechargeable batteries, ACS Catal. 7: 1132-1135, 2017.

[35] P. Kurzweil. Gaston plante and his invention of the lead-acid battery-the genesis of the first practical rechargeable battery, J. Power Sources 195: 4424-4434, 2010.

[36] A. Fernandes, J. C. Afonso and A. J. B. Dutra, Hydrometallurgical route to recover nickel, cobalt and cadmium from spent ni-cd batteries, J. Power Sources 220: 286-291, 2012.

[37] S. R. Ovshinsky, M. A. Fetcenko and J. Ross, A nickel metal hydride battery for electric vehicles, Science 260: 176-181, 1993.

[38] T. Sakai, H. Miyamura, N. Kuriyama, H. Ishikawa and I. Uehara, Rare-earth-based hydrogen storage alloys for rechargeable nickel metal hydride batteries, J. Alloys Compd. 192: 155-157, 1993.

[39] J. M. Tarascon, A. S. Gozdz, C. Schmutz, F. Shokoohi and P. C. Warren, Performance of bellcore's plastic rechargeable Li-ion batteries, Solid State Ionics 86-8: 49-54, 1996.

[40] V. Etacheri, R. Marom, R. Elazari, G. Salitra and D. Aurbach, Challenges in the development of advanced Li-ion batteries: A review, Energy Environ. Sci. 4: 3243-3262, 2011.

[41] L. G. Lu, X. B. Han, J. Q. Li, J. F. Hua and M. G. Ouyang, A review on the key issues for lithium-ion battery management in electric vehicles, J. Power Sources 226: 272-288, 2013.

[42] V. Palomares, P. Serras, I. Villaluenga, K. B. Hueso, J. Carretero-Gonzalez and T. Rojo, Na-ion batteries, recent advances and present challenges to become low cost energy storage systems, Energy Environ. Sci. 5: 5884-5901, 2012.

[43] M. H. Han, E. Gonzalo, G. Singh and T. Rojo, A comprehensive review of sodium layered oxides: powerful cathodes for Na-ion batteries, Energy Environ. Sci. 8: 81-102, 2015.

[44] A. Gurung, K. Chen, R. Khan, S. S. Abdulkarim, G. Varnekar, R. Pathak, R. Naderi and Q. Qiao, Highly efficient perovskite solar cell photocharging of lithium ion battery using DC-DC booster, Adv. Energy Mater.1602105, 2017.

[45] T. L. Gibson and N. A. Kelly, Solar photovoltaic charging of lithium-ion batteries, J. Power Sources 195: 3928-3932, 2010.

[46] J. Xu, Y. Chen and L. Dai, Efficiently photo-charging lithium-ion battery by

perovskite solar cell, Nature Commun. 6: 8103, 2015.

[47] K. Takada, T. Kanbara, Y. Yamanura and S. Kondo, Photo-rechargeable solid state battery, Solid State Ionics 40: 955-958, 1990.

[48] G. Hodes. J. Manassen and D. Cahen, Photoelectrochemical energy conversion and storage using polycrystalline chalcogenide electrodes, Nature 261: 403-404, 1976.

[49] S. Evers, T. Yim and L. F. Nazar, Understanding the nature of absorption/ adsorption in nanoporous polysulfide sorbents for the Li–S battery, J. Phys. Chem. C 116: 19653-19658, 2012.

[50] Z. Wei, D. Liu, C. Hsu and F. Liu, All-vanadium redox photoelectrochemical cell: An approach to store solar energy, Electrochem. Commun. 45: 79-82, 2014.

[51] K. M. Liao, P. Mao, N. Li, M. Han, J. Yi, P. He, Y. Sun and H. S. Zhou, Stabilization of polysulfides via lithium bonds for Li–S batteries, J. Mater. Chem. A 4: 5406-5409, 2016.

[52] G. Zhou, L. Li, D. W. Wang, X. Y. Shan, S. Pei, F. Li and H. M. Cheng, A flexible sulfur-graphene-polypropylene separator integrated electrode for advanced Li-S batteries, Adv. Mater. 27: 641-647, 2015.

[53] P. G. Bruce, S. A. Freunberger, L. J. Hardwick and J. M. Tarascon, Li-O_2 and Li-S batteries with high energy storage, Nature Mater. 11: 19-29, 2011.

[54] F. Wu, J. T. Lee, N. Nitta, H. Kim, O. Borodin and G. Yushin, Lithium iodide as a promising electrolyte additive for lithium-sulfur batteries: mechanisms of performance enhancement, Adv. Mater. 27: 101-108, 2015.

[55] A. Manthiram, Y. Z. Fu, S. H. Chung, C. X. Zu and Y. S. Su, Rechargeable lithium-sulfur batteries, Chem. Rev. 114: 11751-11787, 2014.

[56] L. Wang, J. Liu, S. Yuan, Y. Wang and Y. Xia, To mitigate self-discharge of lithium–sulfur batteries by optimizing ionic liquid electrolytes, Energy Environ. Sci. 9: 224-231, 2016.

[57] N. Li, Y. R. Wang, D. M. Tang and H. S. Zhou, Integrating a photocatalyst into a hybrid lithium-sulfur battery for direct storage of solar energy, Angew. Chem. Int. Ed. 54: 9271-9274, 2015.

[58] S. N. Lou, N. Yap, J. Scott, R. Amal and Y. H. Ng, Influence of MoO_3 (110) crystalline plane on its self-charging photoelectrochemical properties, Sci. Rep. 4: 7428, 2014.

[59] G. Kim, M. Oh and Y. Park, Solar-rechargeable battery based on photoelectrochemical water oxidation: solar water battery, Sci. Rep. 6: 33400, 2016.

[60] R. Thimmappa, B. Paswan, P. Gaikwad, M. C. Devendrachari, H. Makri Nimbegondi Kotresh, R. Rani Mohan, J. Pattayil Alias and M. O. Thotiyl, Chemically chargeable photo battery, J. Phys. Chem. C 119: 14010-14016, 2015.

[61] W. Guo, X. Xue, S. Wang, C. Lin and Z. L. Wang, An integrated power pack of dye-sensitized solar cell and Li battery based on double-sided TiO_2 nanotube arrays, Nano lett. 12: 2520-2523, 2012.

[62] A. Paolella, C. Faure, G. Bertoni, S. Marras, A. Guerfi, A. Darwiche, P. Hovington, B. Commarieu, Z. Wang, M. Prato, M. Colombo, S. Monaco, W. Zhu, Z. Feng, A. Vijh, C. George, G. P. Demopoulos, M. Armand and K. Zaghib, Light-assisted delithiation of lithium iron phosphate nanocrystals towards photo-rechargeable lithium ion batteries, Nat. Commun. 8: 14643, 2017.

[63] J. Xiao, D. Mei, X. Li, W. Xu, D. Wang, G. L. Graff, W. D. Bennett, Z. Nie, L. V. Saraf, I. A. Aksay, J. Liu and J. G. Zhang, Hierarchically porous graphene as a lithium-air battery electrode, Nano lett. 11: 5071-5078, 2011.

[64] J. Yi, Y. Liu, Y. Qiao, P. He and H. Zhou, Boosting the cycle life of $Li–O_2$ batteries at elevated temperature by employing a hybrid polymer–ceramic solid electrolyte, ACS Energy Lett. 2: 1378-1384, 2017.

[65] S. C. Wu, J. Yi, K. Zhu, S. Y. Bai, Y. Liu, Y. Qiao, M. Ishida and H. S. Zhou, A

super-hydrophobic quasi-solid electrolyte for Li-O_2 battery with improved safety and cycle life in humid atmosphere, Adv. Energy Mater. 7: 1601759, 2017.

[66] Y. Chen, S. A. Freunberger, Z. Peng, O. Fontaine and P. G. Bruce, Charging a Li-O_2 battery using a redox mediator, Nature Chem. 5: 489-494, 2013.

[67] M. M. Thackeray, C. Wolverton and E. D. Isaacs, Electrical energy storage for transportation-approaching the limits of, and going beyond, lithium-ion batteries, Energy Environ. Sci. 5: 7854, 2012.

[68] S. A. Freunberger, Y. Chen, N. E. Drewett, L. J. Hardwick, F. Barde and P. G. Bruce, The lithium-oxygen battery with ether-based electrolytes, Angew. Chem. Int. Ed. 50: 8609-8613, 2011.

[69] Y.-C. Lu, D. G. Kwabi, K. P. C. Yao, J. R. Harding, J. Zhou, L. Zuin and Y. Shao-Horn, The discharge rate capability of rechargeable Li–O_2 batteries, Energy Environ. Sci. 4: 2999, 2011.

[70] M. Yu, X. Ren, L. Ma and Y. Wu, Integrating a redox-coupled dye-sensitized photoelectrode into a lithium-oxygen battery for photoassisted charging, Nat. Commun. 5: 5111, 2014.

[71] Y. Zhao, L. N. Wang and H. R. Byon. High-performance rechargeable lithium-iodine batteries using triiodide/iodide redox couples in an aqueous cathode, Nat. Commun. 4: 2013.

[72] Y. Zhao, M. Hong, N. B. Mercier, G. H. Yu, H. C. Choi and H. R. Byon, A 3.5 V lithium-iodine hybrid redox battery with vertically aligned carbon nanotube current collector, Nano lett. 14: 1085-1092, 2014.

[73] F. C. Liu, Z. Shadike, F. Ding, L. Sang and Z. W. Fu, Preferential orientation of I_2-LiI$(HPN)_2$ film for a flexible all-solid-state rechargeable lithium-iodine paper battery, J. Power Sources 274: 280-285, 2015.

[74] Y. Zhao and H. R. Byon, High-performance lithium-iodine flow battery, Adv.

Energy Mater. 3: 1630-1635, 2013.

[75] H. N. Chen and Y. C. Lu, A high-energy-density multiple redox semi-solid-liquid flow battery, Adv. Energy Mater. 6: 2016.

[76] M. Yu, W. D. McCulloch, D. R. Beauchamp, Z. Huang, X. Ren and Y. Wu, Aqueous lithium-iodine solar flow battery for the simultaneous conversion and storage of solar energy, J. Am. Chem. Soc. 137: 8332-8335, 2015.

[77] S. Liao, X. Zong, B. Seger, T. Pedersen, T. Yao, C. Ding, J. Shi, J. Chen and C. Li, Integrating a dual-silicon photoelectrochemical cell into a redox flow battery for unassisted photocharging, Nat. Commun. 7: 11474, 2016.

[78] W. Li, H. C. Fu, L. Li, M. Caban-acevedo, J. H. He and S. Jin, Integrated photoelectrochemical solar energy conversion and organic redox flow battery devices, Angew. Chem. Int. Ed. 55: 13104-13108, 2016.

[79] N. F. Yan, G. R. Li and X. P. Gao. Solar rechargeable redox flow battery based on Li_2WO_4/LiI couples in dual-phase electrolytes, J. Mater. Chem. A 1: 7012, 2013.

[80] B. Lei, G.-R. Li, P. Chen and X.-P. Gao, A solar rechargeable battery based on hydrogen storage mechanism in dual-phase electrolyte, Nano Energy 38: 257-262, 2017.

[81] Y. R. Wang, P. He and H. S. Zhou, Li-redox flow batteries based on hybrid electrolytes: at the cross road between Li-ion and redox flow batteries, Adv. Energy Mater. 2: 770-779, 2012.

[82] K. J. Kim, M.-S. Park, Y.-J. Kim, J. H. Kim, S. X. Dou and M. Skyllas-Kazacos, A technology review of electrodes and reaction mechanisms in vanadium redox flow batteries, J. Mater. Chem. A 3: 16913-16933, 2015.

[83] G. L. Soloveichik, Flow batteries: Current status and trends, Chem. Rev. 115: 11533-11558, 2015.

[84] N. Li, Y. R. Wang, D. M. Tang and H. S. Zhou. Integrating a photocatalyst into a

hybrid lithium-sulfur battery for direct storage of solar energy, Angew. Chem. Int. Ed. 54: 9271-9274, 2015.

[85] M. Kapilashrami, Y. F. Zhang, Y. S. Liu, A. Hagfeldt and J. H. Guo, Probing the optical property and electronic structure of TiO_2 nanomaterials for renewable energy applications, Chem. Rev. 114: 9662-9707, 2014.

[86] S. H. Ge, B. L. Yi and H. M. Zhang, Study of a high power density sodium polysulfide/bromine energy storage cell, J. Appl. Electrochem. 34: 181-185, 2004.

[87] L. H. Wan and Y. M. Xu, Iodine-sensitized oxidation of ferrous ions under UV and visible light: the influencing factors and reaction mechanism, Photochem. Photobiol. 12: 2084-2088, 2013.

[88] C. Barchasz, F. Molton, C. Duboc, J. C. Lepretre, S. Patoux and F. Alloin, Lithium/sulfur cell discharge mechanism: an original approach for intermediate species identification, Anal. Chem. 84: 3973-3980, 2012.

[89] J. K. Hou, J. Song, Y. B. Niu, C. J. Cheng, H. He, Y. T. Li and M. W. Xu, Carbon-coated P2-type $Na_{0.67}Ni_{0.33}Ti_{0.67}O_2$ as an anode material for sodium ion batteries, J. Solid State Electrochem. 19: 1827-1831, 2015.

[90] I. Hasa, S. Passerini and J. Hassoun, A rechargeable sodium-ion battery using a nanostructured Sb-C anode and P2-type layered $Na_{0.6}Ni_{0.22}Fe_{0.11}Mn_{0.66}O_2$ cathode, Rsc Adv. 5: 48928-48934, 2015.

[91] Y. Zhao, L. N. Wang and H. R. Byon, High-performance rechargeable lithium-iodine batteries using triiodide/iodide redox couples in an aqueous cathode, Nat. Commun. 4: 1-7, 2013.

[92] G. Hitoki, A. Ishikawa, T. Takata, J. N. Kondo, M. Hara and K. Domen, Ta_3N_5 as a novel visible light-driven photocatalyst ($\lambda < 600$ nm), Chem. Lett. 736-737, 2002.

[93] M. Tabata, K. Maeda, M. Higashi, D. L. Lu, T. Takata, R. Abe and K. Domen, Modified Ta_3N_5 powder as a photocatalyst for O_2 evolution in a two-step water splitting

system with an iodate/iodide shuttle redox mediator under visible light, Langmuir 26: 9161-9165, 2010.

[94] M. X. Li, W. J. Luo, D. P. Cao, X. Zhao, Z. S. Li, T. Yu and Z. G. Zou, A co-catalyst-loaded Ta_3N_5 photoanode with a high solar photocurrent for water splitting upon facile removal of the surface layer, Angew. Chem. Int. Ed. 52: 11016-11020, 2013.

[95] S. S. Guo, P. Liu, Y. Sun, K. Zhu, J. Yi, M. W. Chen, M. Ishida and H. S. Zhou, A high-voltage and ultralong-life sodium full cell for stationary energy storage, Angew. Chem. Int. Ed. 54: 11701-11705, 2015.

[96] Z. Song, Y. Qian, M. Otani and H. Zhou, Stable Li-organic batteries with nafion-based sandwich-type separators, Adv. Energy Mater. 6: 1501780, 2016.

[97] Z. Q. Jin, K. Xie, X. B. Hong, Z. Q. Hu and X. Liu, Application of lithiated nafion ionomer film as functional separator for lithium sulfur cells, J. Power Sources 218: 163-167, 2012.

[98] I. Bauer, S. Thieme, J. Bruckner, H. Althues and S. Kaskel, Reduced polysulfide shuttle in lithium-sulfur batteries using nafion-based separators, J. Power Sources 251: 417-422, 2014.

[99] Y. L. Wang, Q. L. Sun, Q. Q. Zhao, J. S. Cao and S. H. Ye, Rechargeable lithium/iodine battery with superior high-rate capability by using iodine–carbon composite as cathode, Energy Environ. Sci. 4: 3947, 2011.

[100] X. Su, Q. L. Wu, J. C. Li, X. C. Xiao, A. Lott, W. Q. Lu, B. W. Sheldon and J. Wu, Silicon-based nanomaterials for lithium-ion batteries: a review, Adv. Energy Mater. 4: 2014.

[101] P. P. R. M. L. Harks, F. M. Mulder and P. H. L. Notten, In situ methods for Li-ion battery research: a review of recent developments, J. Power Sources 288: 92-105, 2015.

[102] A. K. Padhi, K. S. Nanjundaswamy and J. B. Goodenough, Phospho-olivines as

positive-electrode materials for rechargeable lithium batteries, J. Electrochem. Soc. 144: 1188-1194, 1997.

[103] Y. G. Wang, Y. R. Wang, E. J. Hosono, K. X. Wang and H. S. Zhou, The design of a $LiFePO_4$/carbon nanocomposite with a core-shell structure and its synthesis by an in situ polymerization restriction method, Angew. Chem. Int. Ed. 47: 7461-7465, 2008.

[104] Y. G. Wang, P. He and H. S. Zhou, Olivine $LiFePO_4$: development and future, Energy Environ. Sci. 4: 805-817, 2011.

[105] Y. H. Huang, H. B. Ren, Z. Peng and Y. H. Zhou, Synthesis of $LiFePO_4$/carbon composite from nano-$FePO_4$ by a novel stearic acid assisted rheological phase method, Electrochim. Acta 55: 311-315, 2009.

[106] J. S. Lee, K. H. You and C. B. Park, Highly photoactive, low bandgap TiO_2 nanoparticles wrapped by graphene, Adv. Mater. 24: 1084-1088, 2012.

[107] S. M. Liu and D. L. He, Low-temperature synthesis of visible light driven TiO_2 microcrystal, Adv. Mater. Res. 512-515: 1927-1932, 2012.

[108] B. Kang and G. Ceder, Battery materials for ultrafast charging and discharging, Nature 458: 190-193, 2009.

[109] A. Tron, Y. N. Jo, S. H. Oh, Y. D. Park and J. Mun, Surface modification of the $LiFePO_4$ cathode for the aqueous rechargeable lithium ion battery, ACS Appl. Mater. Interfaces 9: 12391-12399, 2017.

[110] J. Hassoun, K. S. Lee, Y. K. Sun and B. Scrosati, An advanced lithium ion battery based on high performance electrode materials, J. Mater. Chem. A 133: 3139-3143, 2011.

[111] T. W. Hamann, R. A. Jensen, A. B. F. Martinson, H. Van Ryswyk and J. T. Hupp. Advancing beyond current generation dye-sensitized solar cells, Energy Environ. Sci. 1: 66-78, 2008.

[112] Q. Q. Li, L. L. Lu, C. Zhong, J. Shi, Q. Huang, X. B. Jin, T. Y. Peng, J. G. Qin and

Z. Li, New indole-based metal-free organic dyes for dye-sensitized solar cells, J. Phys. Chem. B 113: 14588-14595, 2009.

[113] A. Mishra, M. K. R. Fischer and P. Bauerle, Metal-free organic dyes for dye-sensitized solar cells: from structure: property relationships to design rules, Angew. Chem. Int. Ed. 48: 2474-2499, 2009.